DOT/FAA/CT-82/150

Atomization and Combustion Performance of Antimisting Kerosene and Jet Fuel

(NASA-CR-174507) ATOMIZATION AND COMBUSTION PERFORMANCE OF ANTIMISTING KEROSENE AND JET FUEL Final Report, Aug. 1981 - Aug. 1982 (Jet Propulsion Lab.) 66 p HC A04/MF A01 CSCL 21D G3/28

N84-16353

Unclas
11438

R. Fleeter
P. Parikh
V. Sarohia

Prepared by
Jet Propulsion Laboratory
California Institute of Technology
Pasadena, California

Prepared for
U.S. Department of Transportation, Federal Aviation Administration
through an agreement with National Aeronautics and Space Administration

December 1983

US Department of Transportation
Federal Aviation Administration
Technical Center
Atlantic City Airport, N.J. 08405

TECHNICAL REPORT STANDARD TITLE PAGE

1. Report No. DOT/FAA/CT-82/150	2. Government Accession No.	3. Recipient's Catalog No.
4. Title and Subtitle Atomization and Combustion Performance of Antimisting Kerosene and Jet Fuel		5. Report Date December 1983 6. Performing Organization Code
7. Author(s) R. Fleeter, P. Parikh and V. Sarohia		8. Performing Organization Report No.
9. Performing Organization Name and Address JET PROPULSION LABORATORY California Institute of Technology 4800 Oak Grove Drive Pasadena, California 91109		10. Work Unit No. 11. Contract or Grant No. DTFA03-80-A-00215 13. Type of Report and Period Covered Final August 1981 - August 1982
12. Sponsoring Agency Name and Address U.S. Department of Transportation Federal Aviation Administration Technical Center Atlantic City, New Jersey 08405		14. Sponsoring Agency Code

15. Supplementary Notes

16. Abstract

Combustion performance of antimisting kerosene (AMK) containing FM-9 polymer developed by ICI-Americas has been investigated at various levels of degradation (restoration of AMK for normal use in a gas turbine engine). To establish the relationship of degradation and atomization to performance in an aircraft gas turbine combustor, sprays formed by the nozzle of a Pratt & Whitney JT8-D combustor with Jet A and AMK at 1 atmosphere (atm) (14.1 lb/in^2 absolute) pressure and 22° C at several degradation levels were analyzed. A new spray characterization technique based on digital image analysis of high resolution, wide field spray images formed under pulsed ruby laser sheet illumination was developed. Combustion tests were performed for these fuels in a JT8-D single can combustor facility to measure combustion efficiency and the lean extinction limit. Correlation of combustion performance under simulated engine operating conditions with nozzle spray Sauter mean diameter (SMD) measured at 1 atm and 22° C has been observed. Fuel spray SMD and hence the combustion efficiency are strongly influenced by fuel degradation level. Use of even the most highly degraded AMK tested (filter ratio = 1.2) resulted in an increase in fuel consumption of 0.08% to 0.20% at engine cruise conditions. A bulk degrader for AMK was built, tested and used to prepare fuel for the combustion tests. The effect of moderate heating of the fuel on degrader performance was also investigated.

17. Key Words (Selected by Author(s))	18. Distribution Statement
Aircraft Fires, Aircraft Safety Antimisting Fuel, Safety Fuel Combustion	

19. Security Classif. (of this report)	20. Security Classif. (of this page)	21. No. of Pages	22. Price
Unclassified	Unclassified		

PREFACE

This report represents the results of research carried out at the Jet Propulsion Laboratory, California Institute of Technology, Contract NAS7-100, Task Order RD-152, Amendment 249 sponsored by the Department of Transportation, Federal Aviation Administration under Agreement No. DTFA03-80-A-00215. The authors extend their gratitude to Mr. Steven Imbrogno, FAA Technical Center, Project Manager for many valuable technical suggestions within the program. The assistance of S. Kikkert in fabrication and assembly of the experimental apparatus is greatly appreciated.

TABLE OF CONTENTS

LIST OF FIGURES

LIST OF FIGURES

LIST OF TABLES

EXECUTIVE SUMMARY

While adoption of antimisting kerosene (AMK) to commercial, turbine powered aircraft applications is motivated by its fire suppression quality, it must be remembered that such a fuel must perform satisfactorily under normal operating conditions in the aircraft gas turbine engine. The ability to atomize and efficiently burn modified fuel in the engine is central to the implementation of AMK and hence to its success in contributing to air transportation safety. The key issue which this study addresses is the relationship of degradation level to engine fuel nozzle atomization performance and to combustion efficiency and stability. Combustion performance is to be related directly to atomization so that new degradation measures and/or new additives which may be devised can be evaluated without undertaking a large scale engine test program. A much better understanding of the reasons behind observed changes in combustion behavior with degradation is also possible when quantitative atomization data are available. Figure E-1 summarizes the relationship of the 3 phases of this approach, degradation, atomization and combustion.

Digital image analysis techniques developed under the FAA sponsored AMK program at JPL (Fleeter et. al., 1982) have been used extensively in the evaluation of atomization performance. Fuel spray drop mean diameters have been measured using these techniques at nozzle flow rates corresponding to ignition, idle, cruise and sea level take-off conditions, using the JT8D-17 dual passage nozzle. The spray atomization tests were carried out with neat Jet A and AMK with post-degradation filter ratios varying from 30 (undegraded) to 2.8 at 1 atm pressure 14.1 lb/in^2 absolute and 22° C. A very strong, direct relationship is shown to exist between atomization and degradation and also between atomization performance and fuel filter ratio. Because of the wide range of drop sizes encountered in these sprays and the non-spherical and often optically cloudy nature of the fuel drops, the image analysis method is believed to be the only suitable technique for accurate analysis of the sprays encountered with the use of AMK.

Degradation was accomplished using the technique devised at Southwest Research Institute (SWRI) (Mannheimer, 1981). The technique involves pumping the fuel through a partially closed needle valve at a pressure drop of ~ 135 atm (2000 lb/in^2). The effect of elevated AMK temperature on degrader effectiveness has been explored. The enhanced degradation available from heating is considerable and should be considered in the development of degradation techniques for actual aircraft. Degradation level measurements were carried out using the RAE devised filter ratio test (Knight, 1981).

Combustion performance was measured in a single can jet combustor apparatus. Measurement of air and fuel flow rates and of exhaust gas hydrocarbon content allowed determination of the fuel combustion efficiency. The tests were carried out at ignition, idle and cruise conditions simulated in the combustor through establishment of specific inlet temperature and air flow rate. Combustion measurements were carried out at each run condition over a range of equivalency ratio. Determination of atomization behavior at the previously used nozzle fuel flow conditions permits direct correlation of combustion and atomization performance. Specifically, combustion efficiency is presented as a function of the spray Sauter mean diameter (SMD).

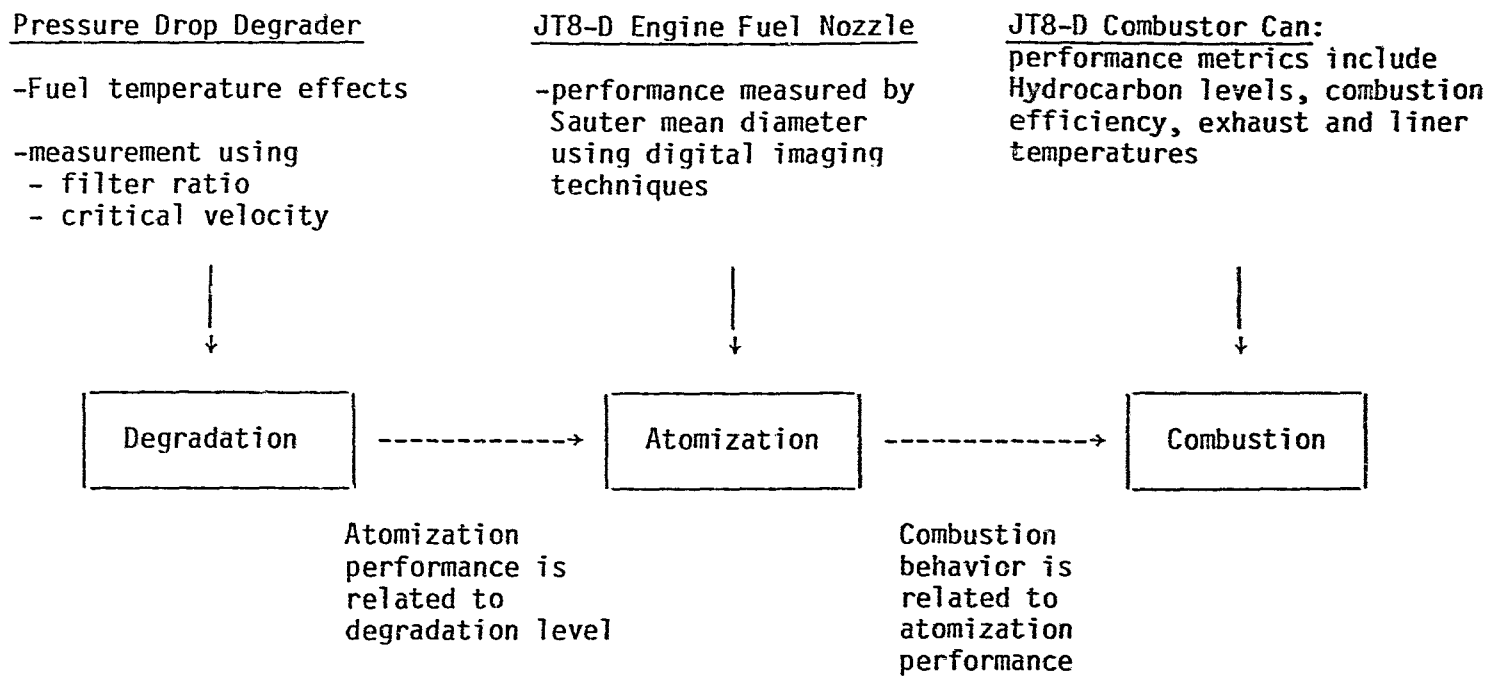

Figure E-1. Organization of the investigation of AMK combustion performance

Combustion performance suffered at idle with increasing SMD and filter ratio, with efficiency dropping from averaged 98.89 +0.10% for Jet A fuel to 97.87 +0.20% for highly degraded AMK (filter ratio 1.2). Less degraded fuel lowered efficiency below 90%. At cruise conditions the loss in efficiency was on the order of 0.10% when switching from Jet A to AMK degraded to filter ratio 1.2. All of these results are in general agreement with those of the British National Gas Turbine Establishment (Lucas Aerospace, 1982) and Pratt and Whitney (Fiorentino et al,. 1980).

The body of this report begins with a brief description of the spray analysis system and the results of the fuel spray characterization study. The combustion tests and their results are then presented along with their analysis in terms of the degradation and fuel atomization results. Significant results of the investigation are highlighted in the Conclusions. Appendices are provided on details of the image analysis system and determination of its accuracy, details of the combustion efficiency calculation, and the effect of fuel heating on degrader performance.

1. FUEL SPRAY CHARACTERIZATION

1.1 Overview

Both the fire safety (flammability) and engine performance (combustion) characteristics of AMK differ from Jet A solely because of its special atomization behavior. Thus it has been felt since the inception of the AMK program that the capability to observe and accurately quantify this aspect of the fuel performance was needed. A spray analysis system which is suited especially to the properties of the fuel sprays encountered was devised, assembled and operated. The system consists of high resolution wide field photography of the spray pattern under pulsed laser sheet illumination and digital analysis of the photographic images thus formed. The requirements of the spray analysis system include the large range of drop sizes to be resolved, the irregular shapes of individual drops, cloudiness of the fuel, high spray density and, particularly ir flammability studies, spray velocity as high as 100 m/s.

Combustion performance evaluation was complemented by results from the spray characterization facility. Sprays formed at simulated ignition, idle, cruise and take-off flow rates at 1 atmosphere pressure 14.1 LB/in^2 absolute and 22° C have been analyzed and spray SMD has been determined. The SMD's were then correlated with combustion performance measured under the same operating conditions.

1.2 Spray Formation, Illumination and Photography

The nozzle spray apparatus (figure 1-1) has been described in detail in earlier work (Reference 1). Essentially it consists of a JT8-D fuel nozzle mounted in a clear enclosure allowing spray illumination and photography. Fuel is fed to the nozzle from pressurized tanks so that flow rates corresponding to engine ignition, idle, cruise and take off may be achieved. Swirl air is also supplied to simulate the environment to which the fuel spray is subjected in the combustor.

Both the illumination and photographic systems remain as described in earlier work (References 1 and 2). They are shown schematically in figure 1-2. The laser, pulsed to 20 ns duration is focused and spread about 1 axis illuminating a cross section of the spray about 1 cm thick. The camera is mounted along an axis perpendicular to this plane. It is fitted with an optical system allowing about a 2:1 ratio of drop to image diameter. High resolution film (Kodak Technical Pan) was used in large format (100 x 120 mm) sheets so that drops as small as 8 μm could be sharply resolved in a spray field of 200 x 240 mm (about 75 square inches). Figure 1-3 shows an entire image recorded in the apparatus of a Jet A fuel spray.

1.3 Image Digitization and Analysis

Analysis of the spray images is accomplished through digitization of portions of the original image and processing of this digital subimage. As this system has evolved considerably since the interim report (Reference 1), it is described in detail in Appendix A. The system is now completely operational on the DEC 11/34/DeAnza ID 5400 system and works interactively with the operator in real time image analysis. All of the results of this section were produced on this minicomputer based system.

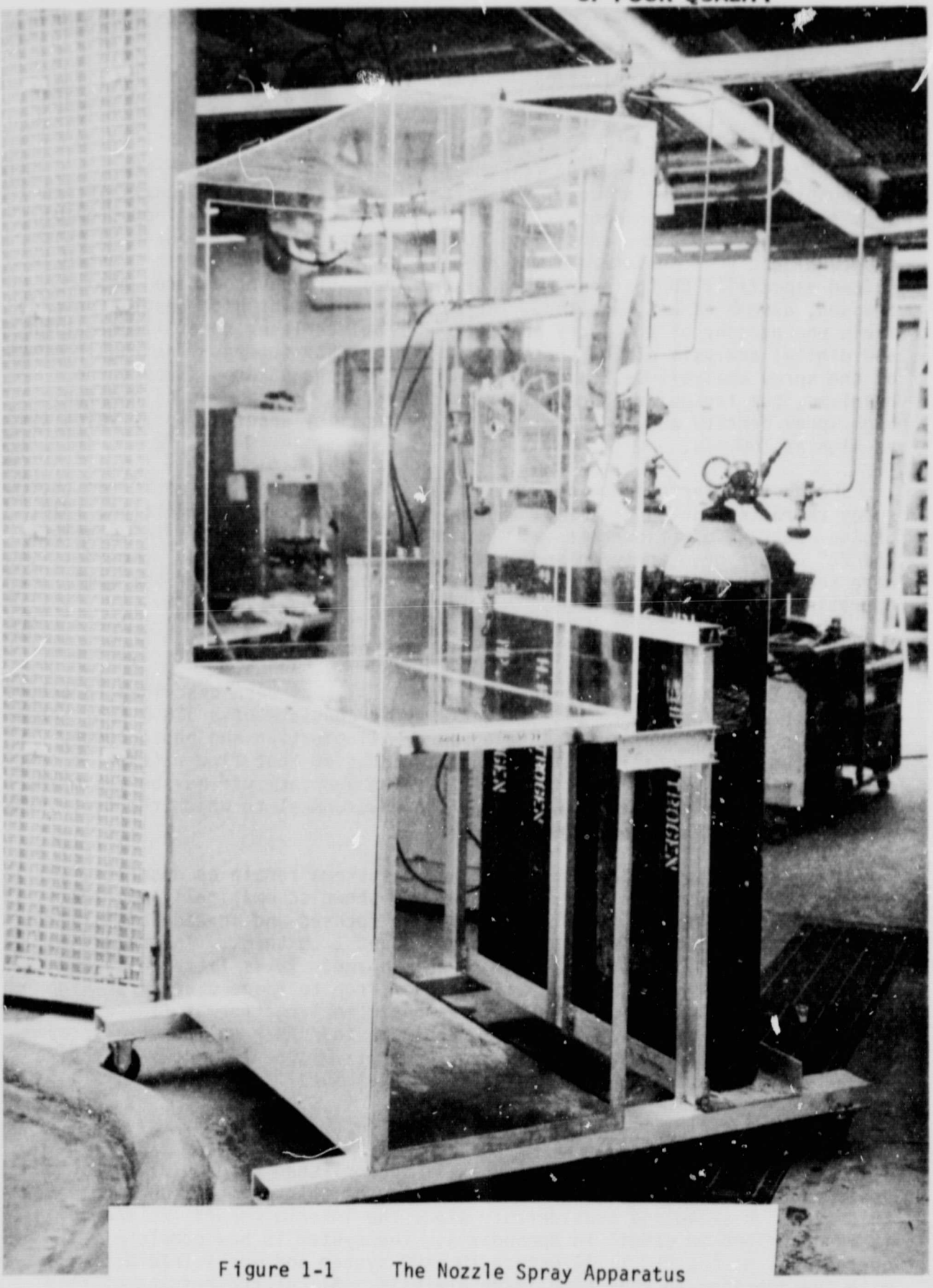

Figure 1-1 The Nozzle Spray Apparatus

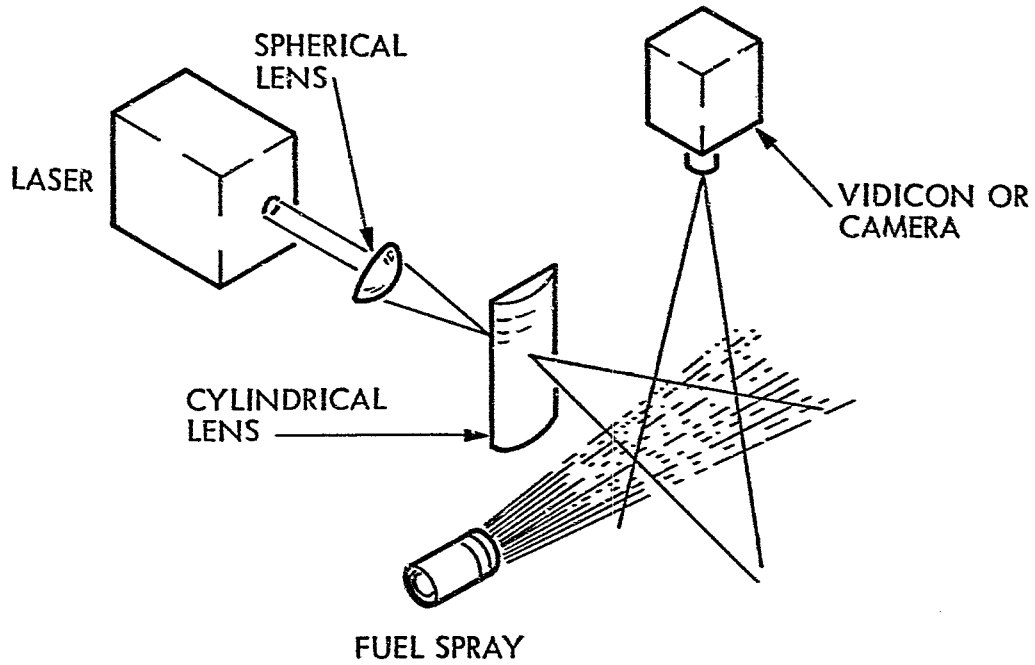

Figure 1-2 SCHEMATIC DIAGRAM OF THE SPRAY ILLUMINATION AND PHOTOGRAPHIC SYSTEMS

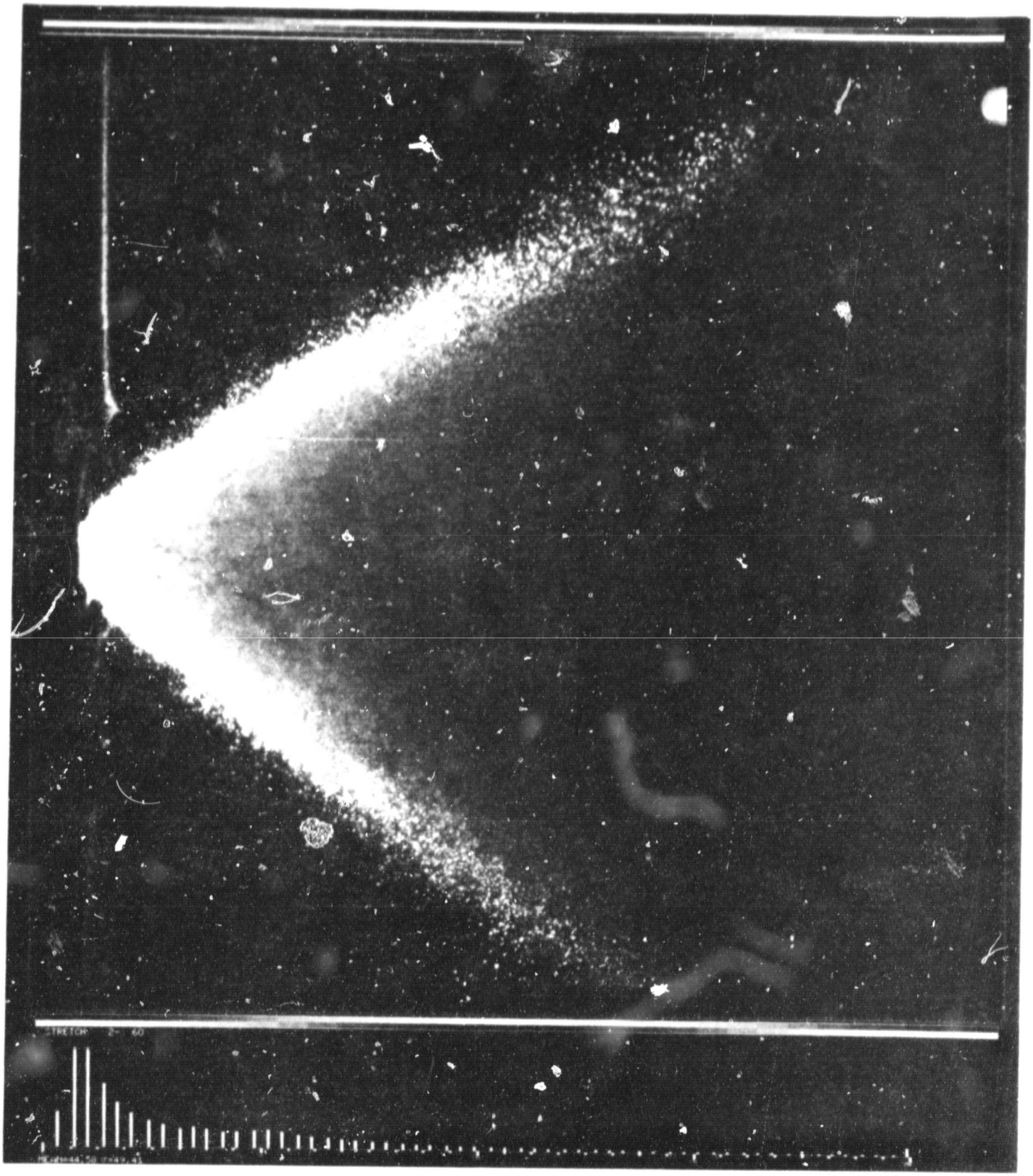

Figure 1-3 A Jet-A Image Formed on a 100mm x 120mm Film Sheet

Upon development of the new system a test of its accuracy was carried out. A sample of glass beads of approximately 130 μm diameter was statistically analyzed both manually and by automated drop counting. This test revealed that the accuracy of the system is at least ±2 percent depending on how much error is assigned to the manual drop counting procedure. The details of this test are discussed in Appendix B.

1.4 Experimental Results and Discussion

The spray measurements described above were undertaken for Jet A, undegraded AMK, and AMK at 3 levels of degradation. Degradation for these tests was accomplished through stirring in an industrial food blender. It should be noted here that degradation of fuel samples for the combustion tests (which were carried out later) were achieved by means of SWRI technique (Reference 3). In both cases the degree of degradation was evaluated by the filter test. There may well be differences in the rheological properties of materials degraded by the two methods to the same filter ratio value. However, such differences were not investigated in the present study. Filter ratios of the fuels tested were 1 (Jet A), 2.8 (90 seconds blender degradation), 4 (30 seconds blender degradation), 5.6 (10 seconds blender degradation) and 30 (undegraded fuel)(the filter ratio test is described in Appendix C). Analysis was carried out at fuel flow rates corresponding to ignition, idle, cruise and sea level take off conditions. The flow rates (m_f) associated with these conditions are summarized in Table 1-1. The nozzle has two orifices denoted primary (pri) and secondary (sec). The secondary nozzle is used to supply additional fuel at the higher flow rates.

Table 1-1. Nozzle Spray Operating Conditions

Operating Condition	$\frac{\dot{m}_f(pri)}{g/s}$	$\frac{\dot{m}_f(sec)}{g/s}$	$\frac{\dot{m}_f(total)}{g/s}$
Ignition	8.5	0	8.5
Idle	16.2	0	16.2
Cruise	18.3	29.9	48.2
Sea Level Take Off	20.3	117	137

For each of the 20 experimental conditions (5 fuel samples x 4 flow rates/sample) spray images were observed for overall changes in characteristics, then analyzed to determine the spray SMD defined as

$$SMD = \frac{\sum D^3}{\sum D^2}$$

where D is the effective drop diameter, determined from the measured cross-sectional area A of a drop using the equation

$$D^2 = \frac{4}{\pi} A$$

This was accomplished through analysis of portions of the fuel spray images at an axial distance of 5 ±0.5 cm from the nozzle exit plane. This location was chosen for consistency with earlier work (Reference 4) and because initial fluid breakup is believed completed at this distance downstream of the ejecting nozzle. Thus, droplet statistics are insensitive to uncertainties in distance measured from the nozzle exit plane at this location. The details of the drop recognition algorithms are described in Appendix A.

Looking at figure 1-3, it is noted that the hollow cone spray produced by the nozzle appears in cross-section as two limbs of atomized fuel. Digital subimages were formed at fixed increments moving radially through the limbs remaining at an axial distance of 5 cm from the nozzle exit plane. A sufficient number of these subimages was formed to count more than 300 individual drops from any single spray. An additional requirement was that the entire limb was traversed in uniform increments in forming subimages so that any spatial variation with radial location would not influence the statistical analysis. The spray cone angle was measured at 2 axial locations.

Spray SMD results and cone angle results are reproduced in Table 1-2. The results are shown graphically in figures 1-4 and 1-5. Note that filter ratio 1 corresponds to neat Jet A and filter ratio 30 to undegraded AMK. Comparing the ignition and idle point atomization results, both of which involve atomization from just the primary nozzle, a significant drop in SMD is evident at the increased flow condition (idle). This is because of the higher pressure drop and fuel exit velocity associated with the increased flow rate. The mean diameter rises again at the cruise condition because of the relatively poor atomization of the secondary nozzle, especially at low flow rates. As expected then, the SMD is lower under take-off conditions as the velocity and pressure drop is increased in the secondary nozzle. The alternating appearance of the curves at higher values of SMD is the result of occasional observation of very large drops ($D > 1000$ μm). Only 3 or 4 of such drops can significantly alter the SMD of a sample containing several hundred drops. These large drops do occur regularly and contain a significant amount of fuel; thus it was felt that they should be included in the sample. However, to produce a curve with less fluctuation, it would be necessary to analyze a much larger portion of the spray or to limit the maximum drop size the system includes in generating statistics. Either of these remedies would serve to secure a sufficiently large sample of drops in any size range to obtain a statistically valid sampling. Thus it is concluded that for the relatively small samples used, accuracy is limited for sprays of SMD greater than 500 to a tolerance of 100 to 200 μm.

Figures 1-6 to 1-9 show a comparison of the present data with results obtained by (Reference 4). At all spray conditions considered, the trends with filter ratio variation are similar but the present results give considerably larger SMD values. This is most likely the result of the limited sensitivity of laser scattering devices such as that used in the Pratt and Whitney study to particles greater than ~ 150 μm diameter. This also explains the complete lack of sensitivity of the Pratt and Whitney results to filter ratio at the take-off condition while the present results show a most striking dependence.

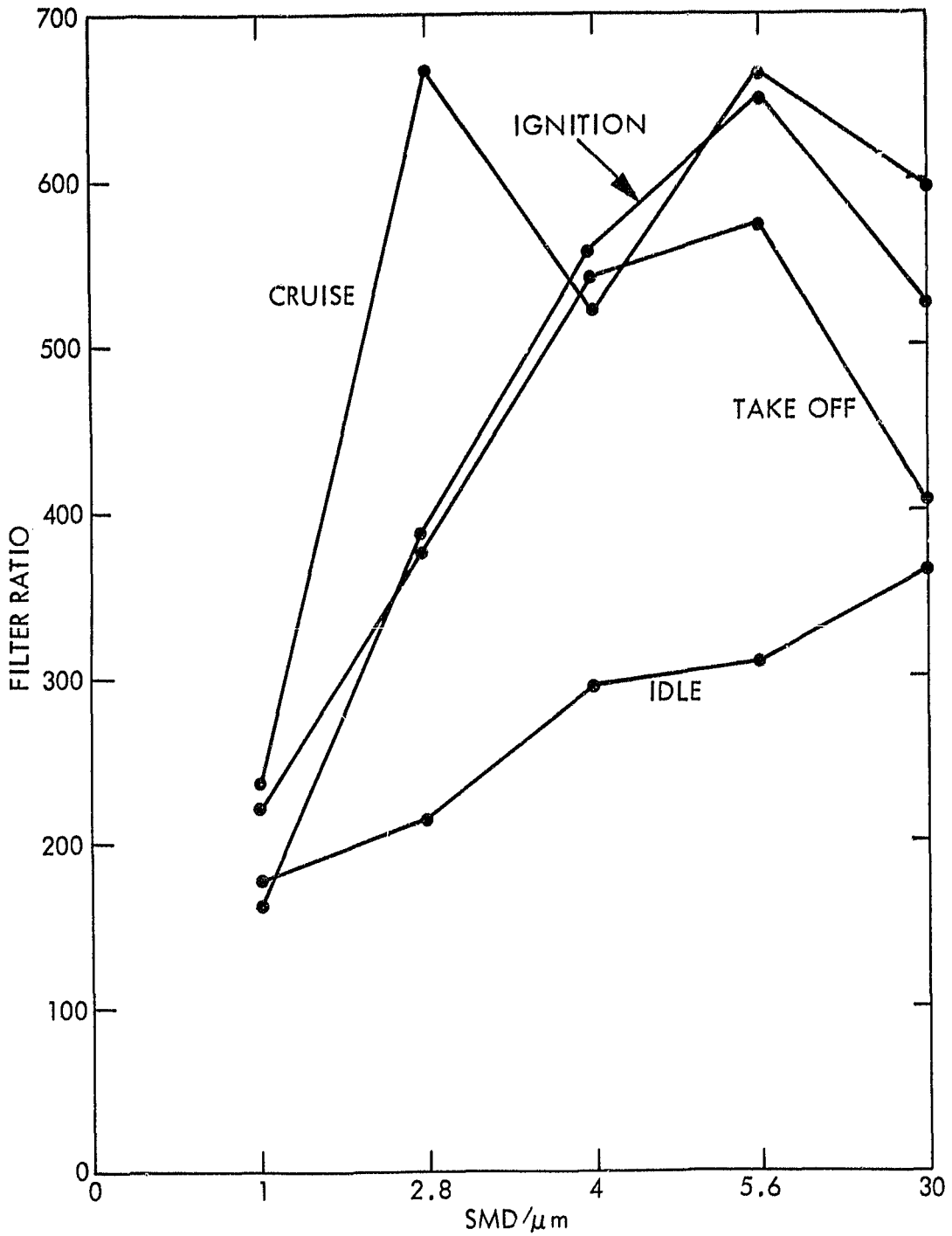

FIGURE 1-4. SPRAY SMD RESULTS

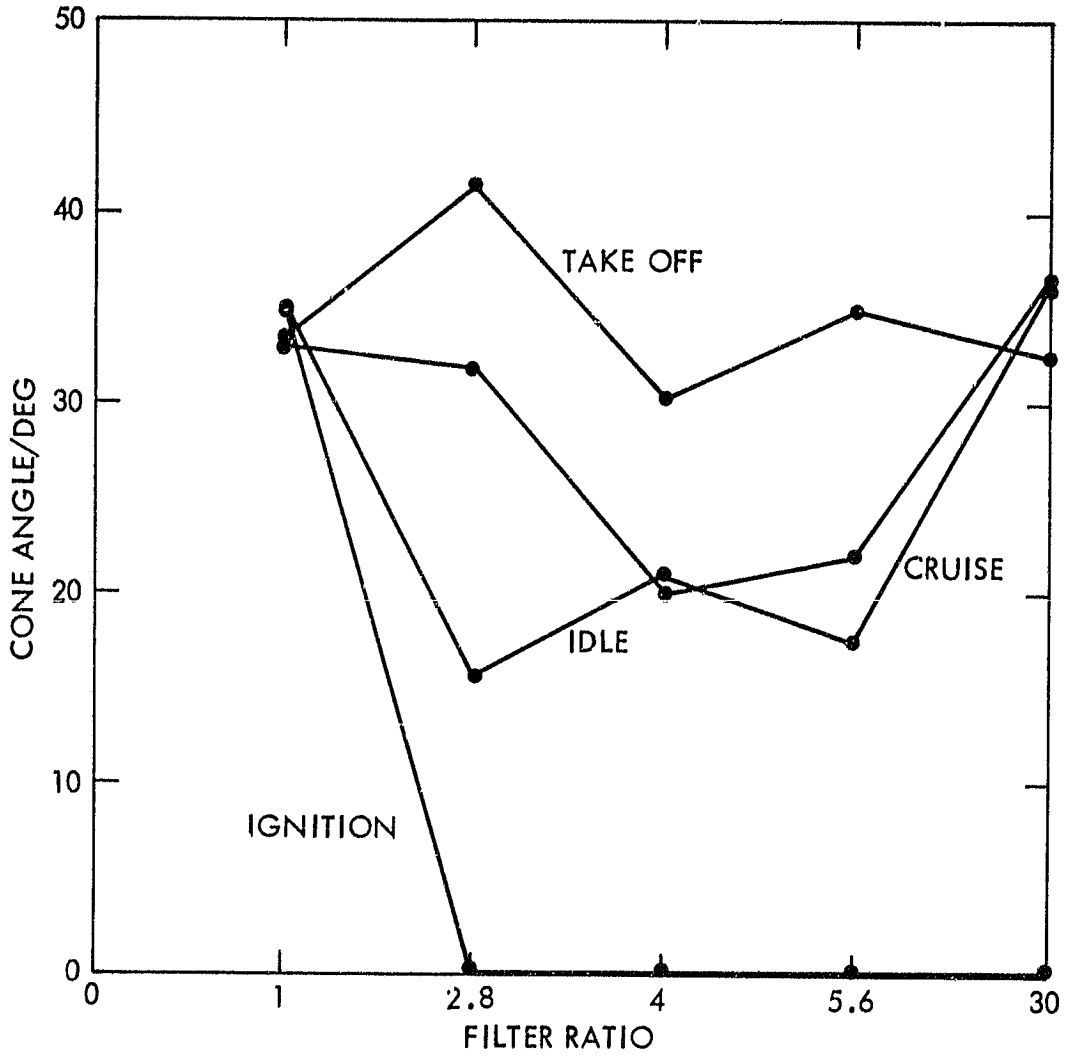

Figure 1-5 SPRAY CONE ANGLE RESULTS

Figures 1-6 through 1-9 also show results obtained using the image analysis system with the maximum drop diameter counted set at 300 and 500 μm.

Table 1-2 Summary of Nozzle Spray Results

Fuel	Filter Ratio	Power Setting	SMD μm	Initial Cone Angle deg.	Final Cone Angle deg.	ΔP_{pri} psi	ΔP_{sec} psi
Jet A	1	Ign.	161	38	32	95	0
		Idle	177	35	27	340	0
		Cruise	236	38	32	440	25
		SLTO	223	39	28	440	140
AMK 90 sec. degraded	2.8	Ign.	390	0*	0*	118	0
		Idle	216	42	22	355	0
		Cruise	664	21	11	440	30
		SLTO	378	43	40	440	180
AMK 30 sec. degraded	4.0	Ign.	561	0*	0*	130	0
		Idle	295	28	16	365	0
		Cruise	519	22	20	440	35
		SLTO	541	36	25	440	200
AMK 10 sec. degraded	5.6	Ign.	651	0*	0*	140	0
		Idle	307	22	22	380	0
		Cruise	664	24	11	440	40
		SLTO	573	35	35	440	220
AMK undegraded	30	Ign.	524	0*	0*	180	0
		Idle	364	47	28	440	0
		Cruise	595	39	35	440	50
		SLTO	405	30	35	440	250

*Cone formation was not observed in these cases. Fuel emerged in long ligaments parallel to the nozzle axis.

For these data, all drops larger than the stated maximum diameter were not included in generation of the spray statistics. This limitation partially simulates the inherent limitation of the Malvern laser analysis system used by (Reference 4). The simulation is not completely rigorous because most laser analysis systems, while they are not inherently sensitive to larger drops, generate statistics assuming a certain number of such drops to be present. The synthetic compensation is based on the size distribution of smaller drops and an assumption of the nature of the entire drop size distribution. Thus a simple size cutoff is not a perfect model of a lower resolution range but synthetically compensated system. However, as is apparent in Figures 1-6 through 1-9, lowering the imaging system dynamic range moves the results towards those obtained with the Malvern system. The measured drop sizes (SMD) are decreased in some cases by as much as 300 μm. More significantly, the drop size dependence on filter ratio is markedly suppressed when larger drops are ignored in generation of spray statistics, exactly as was observed with

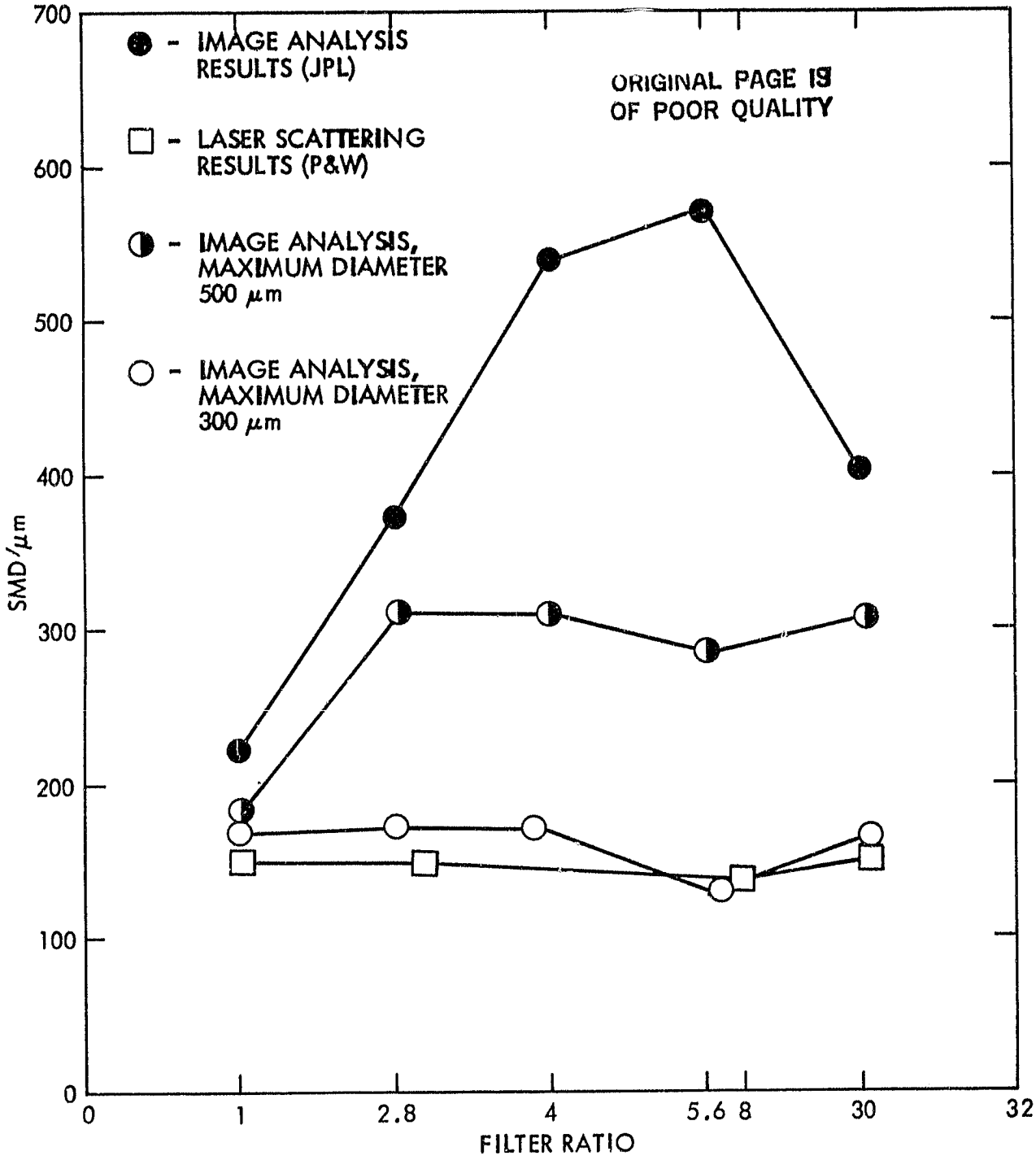

Figure 1-6 COMPARISON OF THE PRESENT RESULTS WITH THE LASER SCATTERING RESULTS OF FIORENTINO (1980) AND WITH IMAGE ANALYSIS RESULTS OBTAINED WITH THE MAXIMUM DROP DIAMETER LIMITED TO 500 μm AND 300μm. TAKEOFF CONDITIONS.

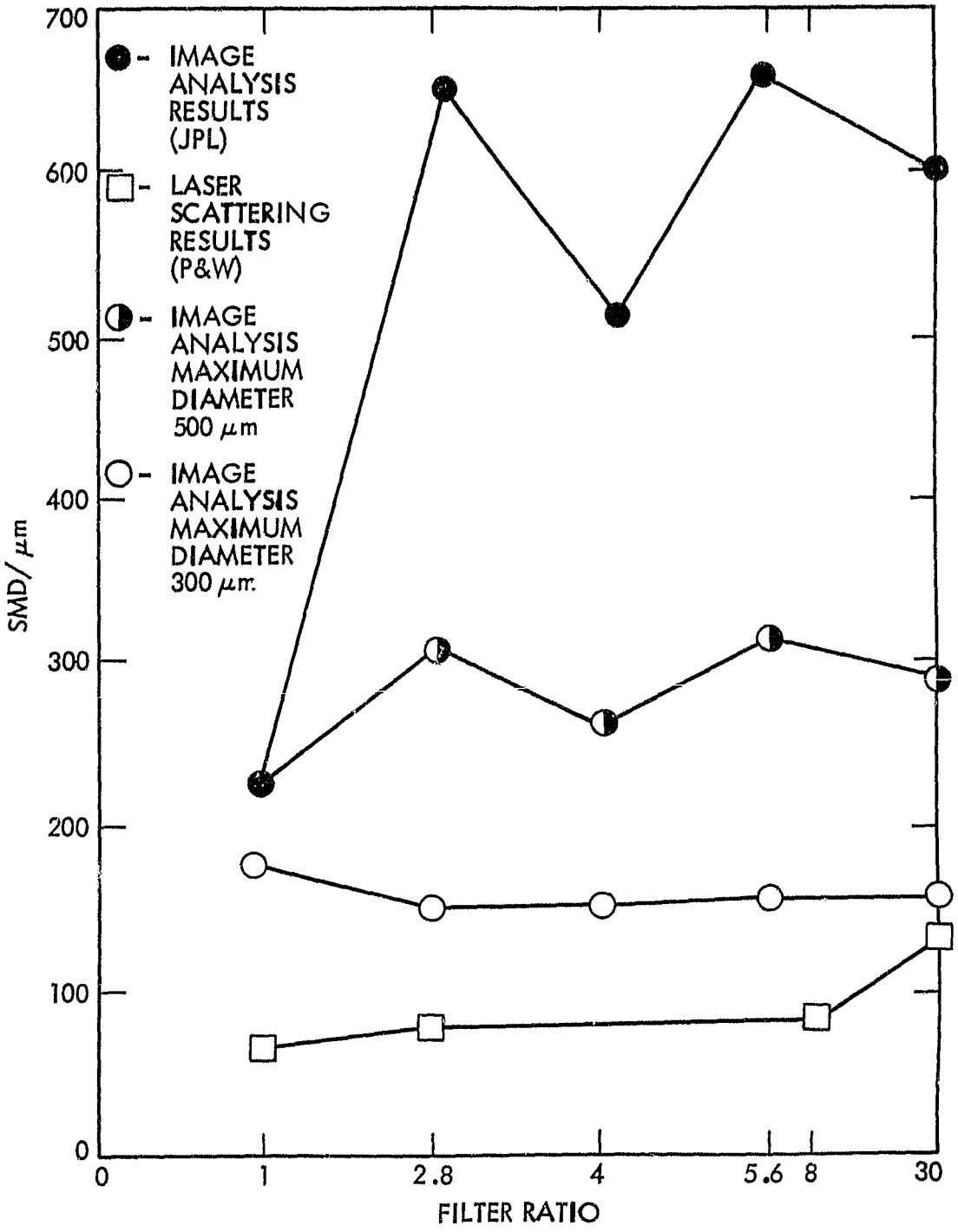

Figure 1-7 COMPARISON OF THE PRESENT RESULTS WITH THE LASER SCATTERING RESULTS OF FIORENTINO (1980) AND WITH IMAGE ANALYSIS RESULTS OBTAINED WITH THE MAXIMUM DROP DIAMETER LIMITED TO 500 μm AND 300μm. CRUISE CONDITIONS.

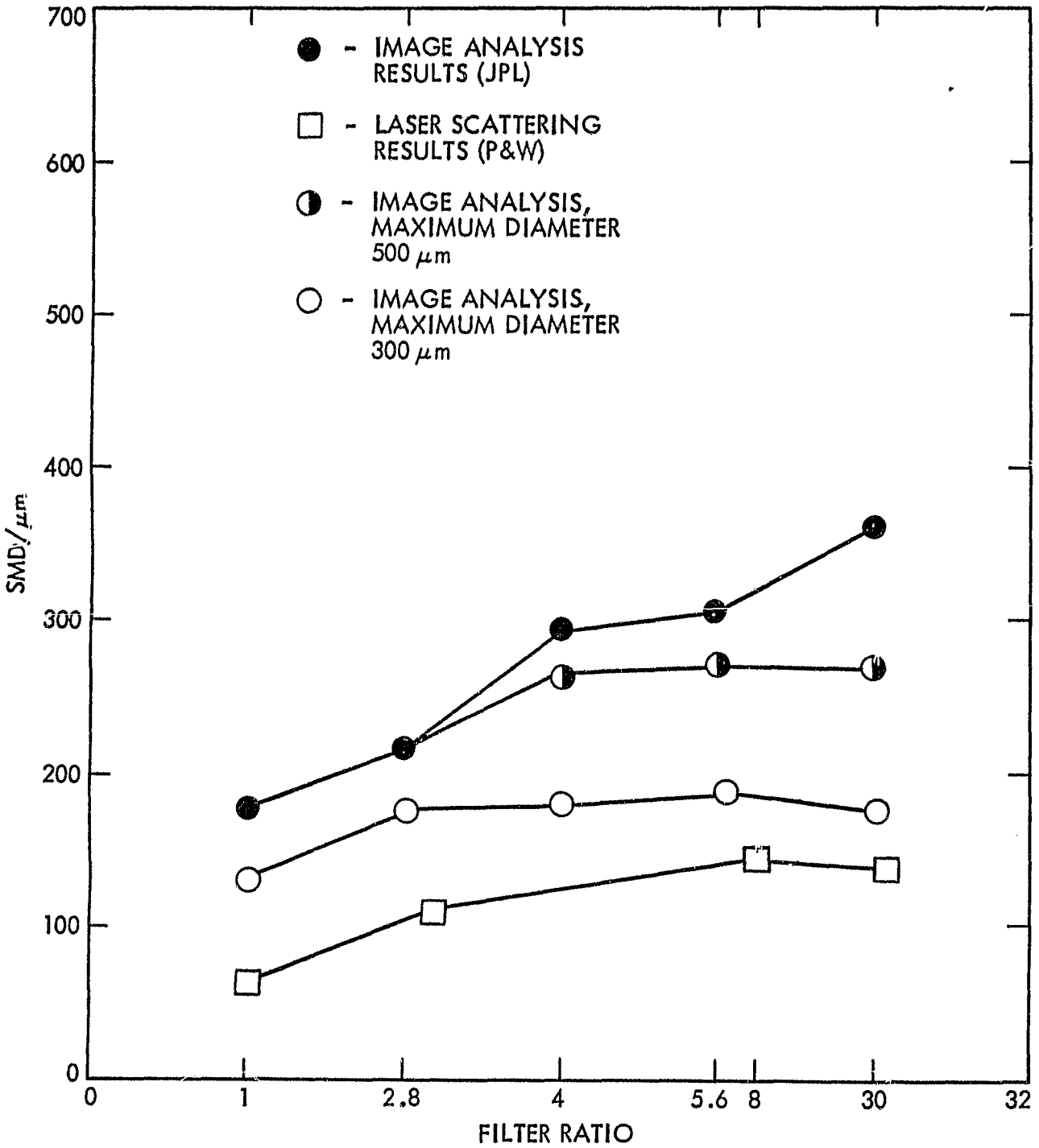

Figure 1-8 COMPARISON OF THE PRESENT RESULTS WITH THE LASER SCATTERING RESULTS OF FIORENTINO (1980) AND WITH IMAGE ANALYSIS RESULTS OBTAINED WITH THE MAXIMUM DROP DIAMETER LIMITED TO 500 μm AND 300 μm. IDLE CONDITIONS.

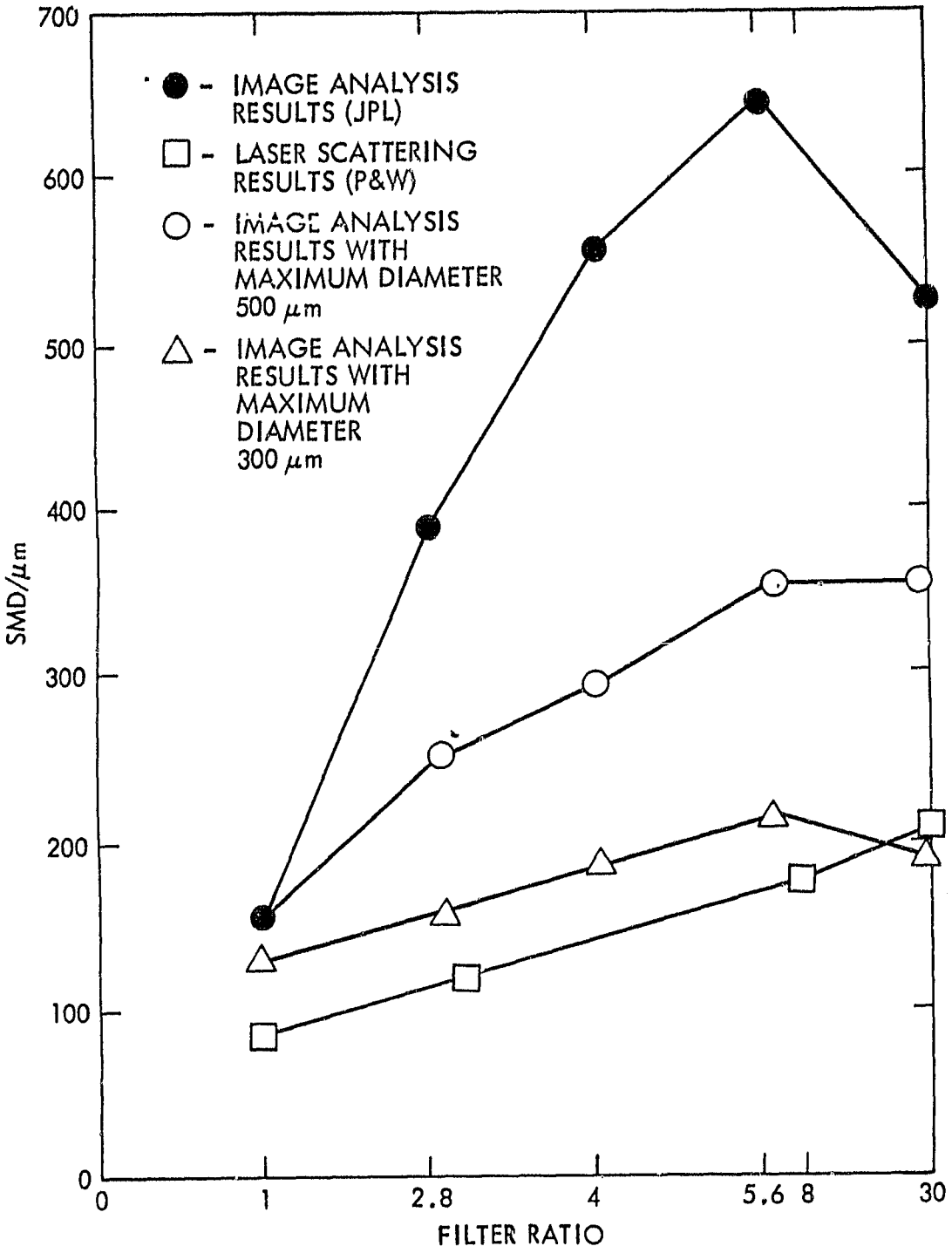

Figure 1-9 COMPARISON OF THE PRESENT RESULTS WITH THE LASER SCATTERING RESULTS OF FIORENTINO (1980) AND WITH IMAGE ANALYSIS RESULTS OBTAINED WITH THE MAXIMUM DROP DIAMETER LIMITED TO 500 μm AND 300 μm. IGNITION CONDITIONS.

the laser scattering data. The scattering data cannot accurately characterize the fuel spray as they apparently account solely for small drops while a very large portion of the fuel is contained in larger drops. For example, a spray composed of 999 drops of 100 μm diameter and 1 drop of 1 mm diameter has 50 percent of its total fuel contained in the single larger drop. Thus any system ignoring these larger drops as the laser system apparently does, is incapable of accurate spray characterization. In the hypothetical case, a laser scattering device would measure the SMD as 100 μm, while the imaging device would record an SMD 81 percent higher (181 μm). This is typical of the discrepancies seen in comparing the present data with laser scattering results.

The dependence of drop size on filter ratio is also demonstrated by figures 1-10 and 1-11. These are the original spray images used for the present analyses of Jet A and undegraded AMK at take off conditions. The Jet A atomization is evidently more extensive than that of AMK, even viewed without magnification as shown in the figures. The Jet A spray is obviously finer and at the measuring point (just left of center at approximately 5 cm from the nozzle) contains virtually no large drops. In comparison the AMK spray is dominated at this point by extremely large fuel masses--many over 1 mm in diameter. The SMD dependence on filter ratio is thus expected to be dramatic. The present data support this expectation while laser scattering data do not (Figure 1-6). As mentioned earlier, the existence of only a few very large drops has a great impact on the spray SMD. The inability of the laser scattering system to discern these very significant fuel masses within the spray results in the discrepancies from the present data.

Figure 1-9 is a comparison of the results at the ignition condition. Again the present data indicate a very much larger SMD than the Pratt and Whitney study. Agreement was only accomplished by limiting counting to drops under 300 μm diameter. The data summary (Table 1-2) shows that no discernable cone of spray was formed by the AMK at any degradation level. In these tests the fluid emerged in a round tube resembling a coiled rope, as shown in figure 1-12. Particle sizes then are of the order of the rope diameter which is of order 1000 μm, in agreement with the present results. It should be pointed out that some smaller particles are evident when the image is viewed under magnification and these result in a slightly diminished SMD. However most of the fuel is contained in the central jet and thus relatively large values of SMD are to be expected.

Except for the idle condition where the fuel is subjected to the highest nozzle pressure drop, the SMD increases quite steeply, progressing from Jet A to the most highly degraded AMK. This tends to suggest that fuel sample may be undergoing further degradation during passage through the nozzle, especially at high nozzle pressure drop condition. The atomization levels achieved by the highly degraded AMK are significantly below those obtained with Jet A and are expected to adversely affect combustion efficiency (see section 2). Thus maximum filter ratios less than 2.8 (or 3 in the case of Pratt and Whitney data) need to be achieved and investigated in the nozzle spray apparatus to gain more information in this area.

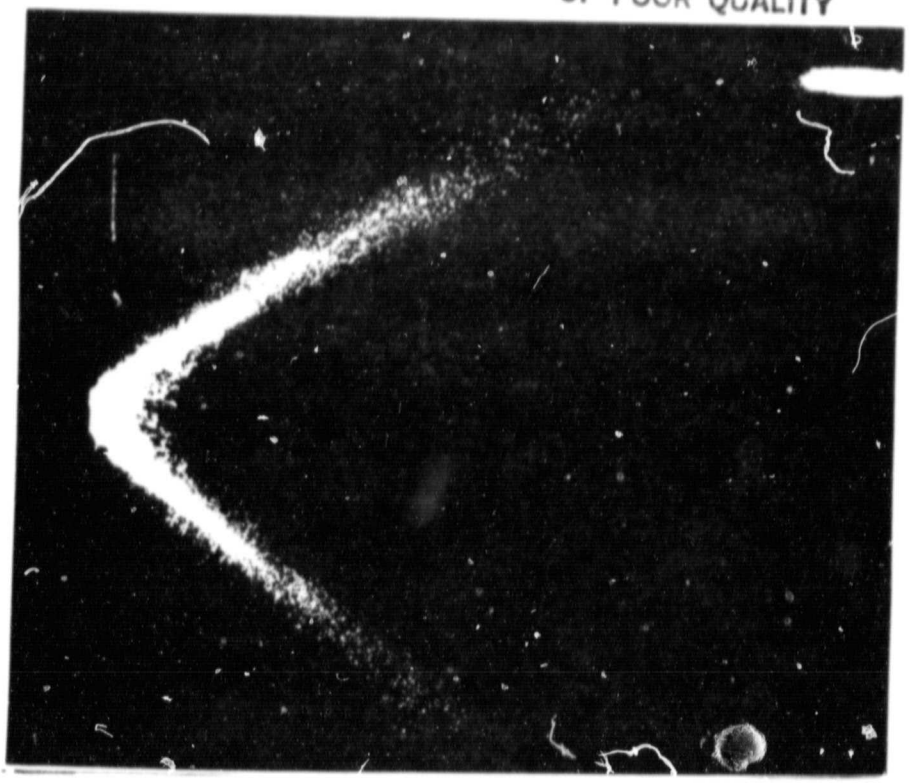

Figure 1-10 ORIGINAL IMAGE OF A JET A FUEL SPRAY AT THE TAKE-OFF CONDITION

Figure 1-11 ORIGINAL IMAGE OF AN UNDEGRADED AMK FUEL SPRAY AT THE TAKE-OFF CONDITION

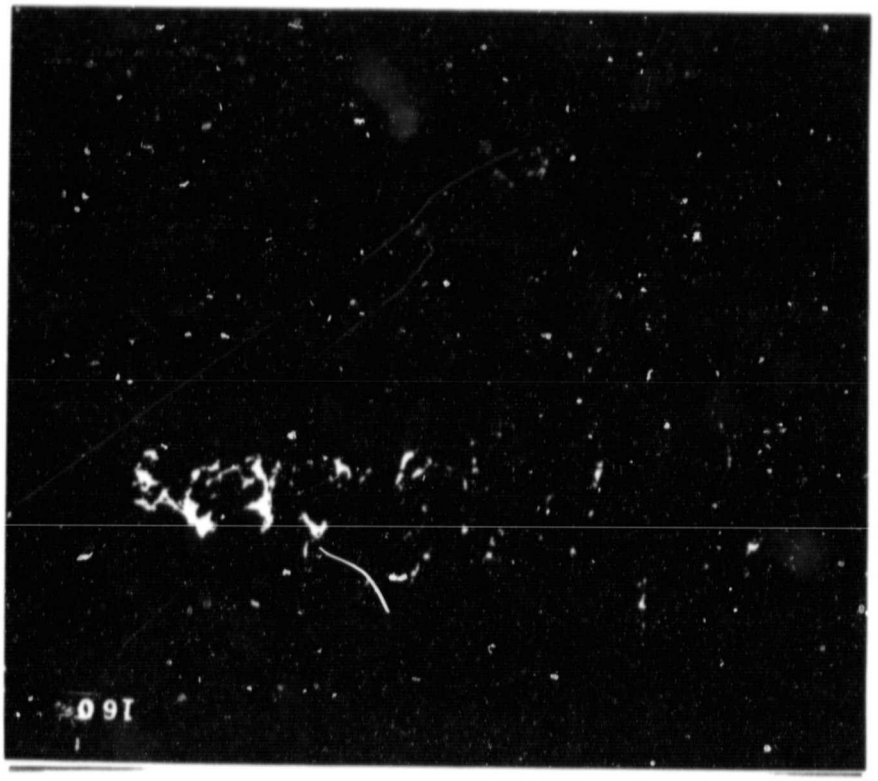

Figure 1-12 ORIGINAL IMAGE OF PARTIALLY DEGRADED (FILTER RATIO 5.6) AMK AT THE IGNITION CONDITION

2. COMBUSTION PERFORMANCE OF ANTIMISTING KEROSENE

2.1 Experimental Apparatus

Combustion performance of AMK over a range of degradation level was measured in the single can jet combustor facility shown schematically in figure 2-1. The facility was fitted with a JT8-D combustor can be supplied by NASA-Lewis Research Center. The can was fitted with the same JT8D-17 dual passage fuel nozzle used for the spray tests reported in section 3 of this report. Through this selection of hardware and appropriate choice of inlet air and fuel flow rates and air temperature, the conditions present in a JT8-D engine combustor were simulated.

Air is supplied to the apparatus from the compressor plant, passing through the 4.3 MW electric heater. Flow metering is accomplished using a sonic nozzle upstream of the plenum. Plenum pressure and temperature are measured and considered as the inlet conditions to the combustor. The fuel to be tested is stored in the pressurized tank. The fuel flows through 9.5 mm (3/8-inch) lines to the primary and secondary nozzle ports. While the fuel system was originally fitted with turbine flow meters, these were subsequently removed because they caused blocking in the flow of AMK. After removal, the flow meters were disassembled and a white, gummy residue was found obstructing the orifice and freezing the turbine motion. This occurred when operating with AMK degraded to filter ratio 6.6 but had not occurred with fuel of filter ratio 1.3. After this test, similar gel deposits were found on a coarse (~ 8 mesh/inch) screen in the fuel line so this device was also removed for all subsequent tests. For the same reason, no fuel pumps were used. Fuel injection was accomplished by pressurization of the fuel tank. Flow rate was then metered with a throttle and determined by measuring the pressure drop across the primary and secondary orifices individually. A calibration of these flow rates as a function of both pressure and degradation level was carried out and reported in detail by Fleeter et al. (Reference 1). Simulation of the turbine section which would be immediately downstream of the combustor in the actual engine is provided by a choked orifice at the rear of the combustor. Part of this orifice is formed by a water cooled gas sample probe which is located along the centerline of the exhaust nozzle. This probe quenches the sampled gas so that reactions are frozen at the exhaust plane and do not continue in the sampling line. To prevent distillation of higher molecular weight constituents of the exhaust, the gas sample line is heated to 200° C along its entire length beginning at the sampling probe exit. The probe is also fitted with a thermocouple, raised on insulating material 3 mm above the probe surface for the measurement of exhaust gas temperature. Thermocouples were also fitted to the combustor liner to measure any effect AMK might have on the liner temperature.

The major effect of the antimisting additive on fuel performance is due not to the chemistry of the additive but to its rheological effect. This is because the additive is introduced at very low concentrations (0.30 percent) and consists mostly of hydrogen and carbon. Thus the aim of this phase of the program was to determine what effect the reduced atomization would have on combustion efficiency. The presence of larger drops would doubtless slow the fuel's evaporation and, since residence time in the combustor is limited, would result in unburned and partially burned fuel appearing in the exhaust. The sampled exhaust gas was therefore introduced into a hydrocarbon analyzer

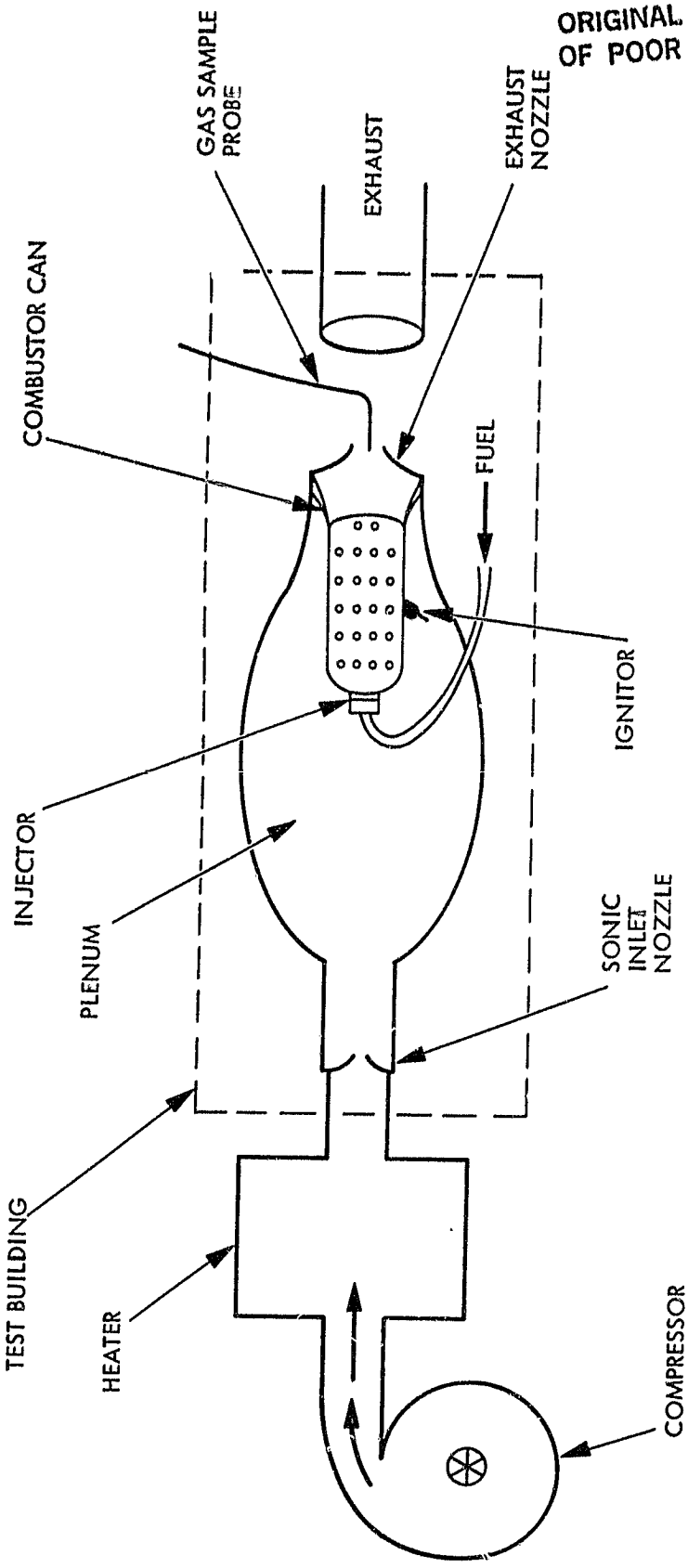

Figure 2-1 SCHEMATIC DIAGRAM OF THE JET COMBUSTOR FACILITY

Table 2-2. Combustor Test Data: Jet A, Filter Ratio = 1

Engine Condition	$\dot{m}_a$ kg/s	$\dot{m}_f$ g/s	A/F Ratio	ϕ	P_{plenum} atm	T_{plenum} °C	T_{liner} °C	EGT °C	HC ppm	η_c %
Idle	1.38	18.8	73.4	0.201	7.17	121	390	630	34	99.26
	1.39	16.1	86.3	0.172	6.88	124	360	560	35	99.10
	1.39	11.0	126	0.117	6.31	120	285	423	33	98.77
	1.39	8.3	167	0.088	5.96	119	247	350	38	98.12
Cruise	2.43	40.9	59.4	0.250	14.2	357	708	*	14	99.75
	2.43	36.7	66.2	0.225	13.8	357	681	*	13	99.74
	2.43	36.0	67.5	0.219	13.7	358	665	*	13	99.74
	2.43	30.5	79.7	0.186	13.3	359	639	*	12	99.72
	2.43	17.7	138	0.108	12.0	358	524	*	13	99.47

*Exhaust gas temperature data not available for these runs.

Table 2-3. Combustor Test Data: AMK, Filter Ratio = 1.2

Engine Condition	$\dot{m}_a$ kg/s	$\dot{m}_f$ g/s	A/F Ratio	ϕ	P_{plenum} atm	T_{plenum} °C	T_{liner} °C	EGT °C	HC ppm	η_c %
Idle	1.28	17.1	74.9	0.200	6.53	142	408	606	44	99.02
	1.28	15.2	84.2	0.176	6.34	141	380	555	55	98.63
	1.28	12.2	105	0.140	5.99	135	331	465	70	97.82
	1.28	9.2	139	0.106	5.67	132	282	380	72	97.03
	1.30	9.2	141	0.105	5.66	122	274	370	77	96.78
	1.30	9.1	143	0.104	*	145	302	385	70	97.03
	1.29	6.8	189	0.078	5.45	120	238	186	70	96.08
Cruise	2.39	58.2	41.1	0.361	14.8	360	791	1089	24	99.71
	2.39	47.1	50.7	0.292	14.0	352	713	960	22	99.67
	2.40	28.6	83.9	0.176	12.6	354	599	714	18	99.55
	2.41	21.2	114	0.130	12.3	356	564	650	20	99.32
	2.39	17.1	140	0.106	11.7	360	519	600	24	99.00
	2.44	17	144	0.103	12.0	367	531	591	18	99.23

*Plenum pressure datum not available for this run.

Table 2-4. Combustor Test Data: AMK, Filter Ratio = 1.3

Engine Condition	$\dot{m}_a$ kg/s	$\dot{m}_f$ g/s	A/F Ratio		P_{plenum} atm	T_{plenum} °C	T_{liner} °C	EGT °C	HC ppm	$\frac{c}{\%}$
Idle	1.39	19	73	0.20	7.2	123	460	670	86	98.14
	1.39	17	82	0.18	7.0	123	410	605	86	97.91
	1.39	12	116	0.13	6.5	124	320	455	77	97.35
	1.39	8	174	0.09	6.0	125	265	343	80	95.87
	1.39	7	199	0.07	5.6	122	250	310	82	95.16
	1.39	5	278	0.05	5.6	125	230	280	92	92.42

Table 2-5. Combustor Test Data: AMK, Filter Ratio = 1.5

Engine Condition	$\dot{m}_a$ kg/s	$\dot{m}_f$ g/s	A/F Ratio	ϕ	P_{plenum} atm	T_{plenum} °C	T_{liner} °C	EGT °C	HC ppm	η_c %
Idle	1.32	20	66.0	0.224	6.0	124	305	400	95	98.14
	1.32	18	73.3	0.202	5.9	123	295	375	96	97.91
	1.32	16	82.5	0.180	5.7	123	275	375	98	97.60
	1.32	15	88.0	0.168	5.4	124	240	386	95	97.52
	1.32	15	88.0	0.168	5.7	123	275	345	95	97.52
	1.32	11.5	115	0.129	5.4	123	243	285	95	96.76
Cruise	2.39	57	41.9	0.353	14.6	354	790	980	41	99.49
	2.39	38	62.9	0.235	14.0	361	745	910	41	99.24
	2.41	29	83.1	0.178	13.2	359	676	800	43	98.94
	2.41	19.5	123	0.120	11.2	356	488	530	44	98.40
	2.40	19.5	123	0.120	11.3	347	480	515	38	98.61
	2.41	17.0	142	0.104	10.9	349	448	475	47	98.02

Table 2-6. Combustor Test Data: AMK, Filter Ratio = 1.6

Engine Condition	$\dot{m}_a$ kg/s	$\dot{m}_f$ g/s	A/F Ratio	ϕ	P_{plenum} atm	T_{plenum} °C	T_{liner} °C	EGT °C	HC ppm	η_c %
Idle	1.29	32.4	39.8	0.372	7.8	131	570	945	30	99.65
	1.29	25.0	51.6	0.287	7.2	130	500	785	35	99.46
	1.29	17.6	73.3	0.203	6.7	129	400	633	39	99.15
	1.29	17.4	74.1	0.200	6.7	130	400	632	34	99.25
	1.29	15.2	84.9	0.175	6.4	129	363	575	48	98.79
	1.29	12.5	103	0.145	6.1	128	335	490	62	98.11
	1.29	10.5	123	0.121	5.9	128	304	433	70	97.45
	1.29	8.8	147	0.102	5.7	130	280	390	64	97.21
	1.30	8.7	150	0.099	5.7	126	273	375	66	97.06
	1.29	6.4	202	0.074	5.4	127	245	325	64	96.17

Table 2-7. Combustor Test Data: AMK, Filter Ratio = 6.6

Engine Condition	$\dot{m}_a$ kg/s	$\dot{m}_f$ g/s	A/F Ratio	ϕ	P_{plenum} atm	T_{plenum} °C	T_{liner} °C	EGT °C	HC ppm	η_c %
Idle	1.32	15.5	85.2	0.174	6.3	125	342	500	145	96.34
	1.32	15.3	86.3	0.172	6.4	125	343	500	135	96.55
	1.32	15.0	88.0	0.168	6.3	125	338	417	160	95.82
	1.32	14.0	94.3	0.157	6.0	124	302	523	170	95.25
	1.32	13.5	97.8	0.151	5.9	124	282	380	160	95.36
	1.32	13.0	102	0.146	6.0	124	304	390	195	94.10
Cruise	2.51	94	26.7	0.555	12.9	323	570	585	50	99.60
	2.50	54	46.3	0.320	12.5	325	546	605	49	99.33
	2.50	34	73.5	0.201	12.4	326	534	645	49	98.93

Table 2-8. Combustor Test Data: AMK, Filter Ratio = 20

Engine Condition	$\dot{m}_a$ kg/s	$\dot{m}_f$ g/s	A/F Ratio	ϕ	P_{plenum} atm	T_{plenum} °C	T_{liner} °C	EGT °C	HC ppm	η_c %
Idle	1.33	12.5	106	0.140	6.2	127	330	450	160	94.97
	1.33	12.0	111	0.133	6.0	124	305	415	168	94.47
	1.33	11.0	121	0.121	5.6	127	270	335	220	92.11
	1.33	10.0	133	0.111	5.4	127	250	280	248	90.22
Cruise	2.41	128	19	0.780	12.6	348	602	700	64	99.64
	2.40	127	19	0.780	14.1	346	700	885	79	99.55
	2.42	94	26	0.570	12.3	347	640	605	61	99.53
	2.36	12	197	0.075	10.9	348	456	505	75	95.62
	2.42	12	202	0.073	10.9	347	500	465	70	95.81

Table 2-9 Jet Combustor Data Summary

Idle Conditions

Fuel	Filter Ratio	ϕ	EGT °C	T_{liner} °C	HC ppm	η_c %
Jet A	1	0.10	380	263	36	98.39 ±0.16
		0.13	455	302	33	98.85 ±0.11
		0.16	530	343	35	99.03 ±0.10
		0.20	630	390	34	99.26 ±0.07
AMK	1.2	0.10	330	270	72	96.65 ±0.35
		0.13	440	315	70	97.59 ±0.25
2 pass @ 2000		0.16	515	360	62	98.27 ±0.15
		0.20	605	410	44	99.02 ±0.10
AMK	1.3	0.10	370	280	79	96.24 ±0.35
		0.13	455	320	77	97.35 ±0.25
1 pass @ 2000		0.16	545	375	82	97.69 ±0.20
		0.20	670	460	86	98.14 ±0.20
AMK	1.5	0.10	260	230	95	96.19 ±0.35
		0.13	285	245	95	96.77 ±0.30
1 pass @ 1000		0.16	310	255	95	97.36 ±0.25
		0.20	375	295	96	97.88 ±0.20
AMK	1.6	0.10	375	275	66	97.06 ±0.30
		0.13	455	315	67	97.70 ±0.25
3 pass @ 2000		0.16	535	350	55	98.45 ±0.15
		0.20	635	400	36	99.25 ±0.10
AMK	6.6	0.10	220	200	*	*
		0.13	320	250	204	92.85 ±0.70
Douglas test degraded only		0.16	430	315	162	95.41 ±0.45
		0.20	580	405	107	*
AMK	20	1.0	220	230	280	89.02 ±1.0
		1.3	395	295	181	91.43 ±0.85
		1.6	575	385	84	*
		2.0	*	*	*	*

*Because of the limited range of ϕ achieved in testing (see text) these data could not be calculated without considerable extrapolation of experimental results.

Table 2-10 Jet Combustor Data Summary

Cruise Conditions

Fuel	Filter Ratio	ϕ	EGT °C	T_{liner} °C	HC ppm	η_c %
Jet A	1	0.10	*	510	13	99.44 ±0.05
		0.13	*	555	12	99.52 ±0.04
		0.16	*	600	12	99.64 ±0.03
		0.20	*	650	13	99.73 ±0.03
		0.25	*	708	14	99.75 ±0.02
		0.30	*	735	15	99.77 ±0.02
AMK	1.2	0.10	580	520	21	99.20 ±0.08
		0.13	650	564	20	99.32 ±0.07
		0.16	690	585	19	99.47 ±0.05
		0.20	765	625	18	99.57 ±0.04
		0.25	870	670	21	99.61 ±0.04
		0.30	975	720	22	99.67 ±0.03
AMK	1.5	0.10	465	440	48	97.92 ±0.20
		0.13	570	515	41	98.58 ±0.15
		0.16	715	615	42	98.80 ±0.10
		0.20	840	705	42	99.06 ±0.10
		0.25	920	750	41	99.27 ±0.07
		0.30	950	770	41	99.38 ±0.06
AMK	6.6	0.10	**	**	**	**
		0.13	**	**	**	**
		0.16	580	530	49	98.79 ±0.10
		0.20	585	535	49	98.93 ±0.10
		0.25	595	540	49	99.01 ±0.10
		0.30	600	540	49	99.26 ±0.07
AMK	20	0.10	490	580	72	95.91 ±0.40
		0.13	490	490	71	96.14 ±0.40
		0.16	490	500	71	96.37 ±0.35
		0.20	510	515	70	96.68 ±0.35
		0.25	530	530	69	97.06 ±0.30
		0.30	540	545	67	97.45 ±0.25

* EGT data not available for these runs.

**Limitation on the range of ϕ achieved in these tests (see text) prohibited calculation of these data without considerable extrapolation of experimental results.

Figures 2-2 and 2-3 show the raw hydrocarbon emissions data obtained at idle and cruise conditions. As anticipated, decreasing filter ratio corresponds to decreasing emissions due to enhanced atomization at higher degradation. Jet A tests are represented as "filter ratio = 1". The one exception to this trend is for the sample with a filter ratio of 1.6. This sample was actually the most highly degraded of all, having been passed through the degrader 3 times, each at a pressure drop of 135 atm (2000 lb/in^2). The sample was found to be very cloudy and it is suspected that the fuel contacted bulk water. Contact of the FM-9 additive with water results in increased filter ratio test results over that which would be expected based on fuel degradation alone. Except at very high filter ratio, hydrocarbon emissions are not strongly affected by the equivalency ratio over the range examined. At higher filter ratios (FR 6.6 and 20), increased size of fuel droplets in the spray results in incomplete evaporation and combustion of the fuel droplets within the combustor. This leads to significantly higher hydrocarbon emissions in the exhaust, especially at low equivalence ratios. However, as the equivalence ratio is increased, the total heat release in the combustor is also increased, leading to a more complete evaporation and combustion of even the higher filter ratio (FR 6.6 and 20) fuels.

Figures 2-4 and 2-5 show the calculated combustion efficiency as a function of filter ratio for idle and cruise conditions, respectively. The increased efficiency with increased ϕ for every fuel is a natural result of lean overall combustion conditions. The cost in efficiency is most dramatic at idle where over 1 percent of efficiency is lost going from Jet A to highly degraded AMK. Smaller but perhaps more significant are the losses observed at cruise conditions. Here losses associated with the change from Jet A to AMK of filter ratio 1.2 range from 0.10 percent to 0.25 percent depending on ϕ. Assuming an engine combustor efficiency loss of 0.10 percent, 50 kg of extra fuel will need to be carried for every 5000 kg of fuel used at cruise with Jet A to make up for the inefficiency. This represents a significant weight and cost penalty associated with the use of AMK. The uncertainty bounds indicated for η_c were calculated based on a combined uncertainty of ±10% in the measurement of m_a, m_f and fractional hydrocarbon content.

Figure 2-6 illustrates the comparison of the present results at simulated idle conditions with those of Rolls Royce (Reference 5) and Pratt & Whitney (Reference 4). The present results are similar to those of Lucas considering that two different combustors were used for the two sets of results (present results are from a single JT8-D combustor can; Lucas results are from an 80° sector of a Rolls Royce RB211 annular combustor). The Pratt & Whitney results also are quantitatively similar and show similar trends. They differ mainly in their low η_c for Jet A. It is noted that the Lucas data show increasing η_c with increasing ϕ in agreement with the present results. The Pratt & Whitney data were presented for only one fuel/air ratio.

The lean limit was also investigated as a measure of fuel atomization performance. Tests were carried out at engine ignition conditions (nominal air flow 0.620 kg/s, inlet temperature 160° C) and involve gradually reducing the fuel flow rate until combustion ceases. Test results are reported in Table 2-11.

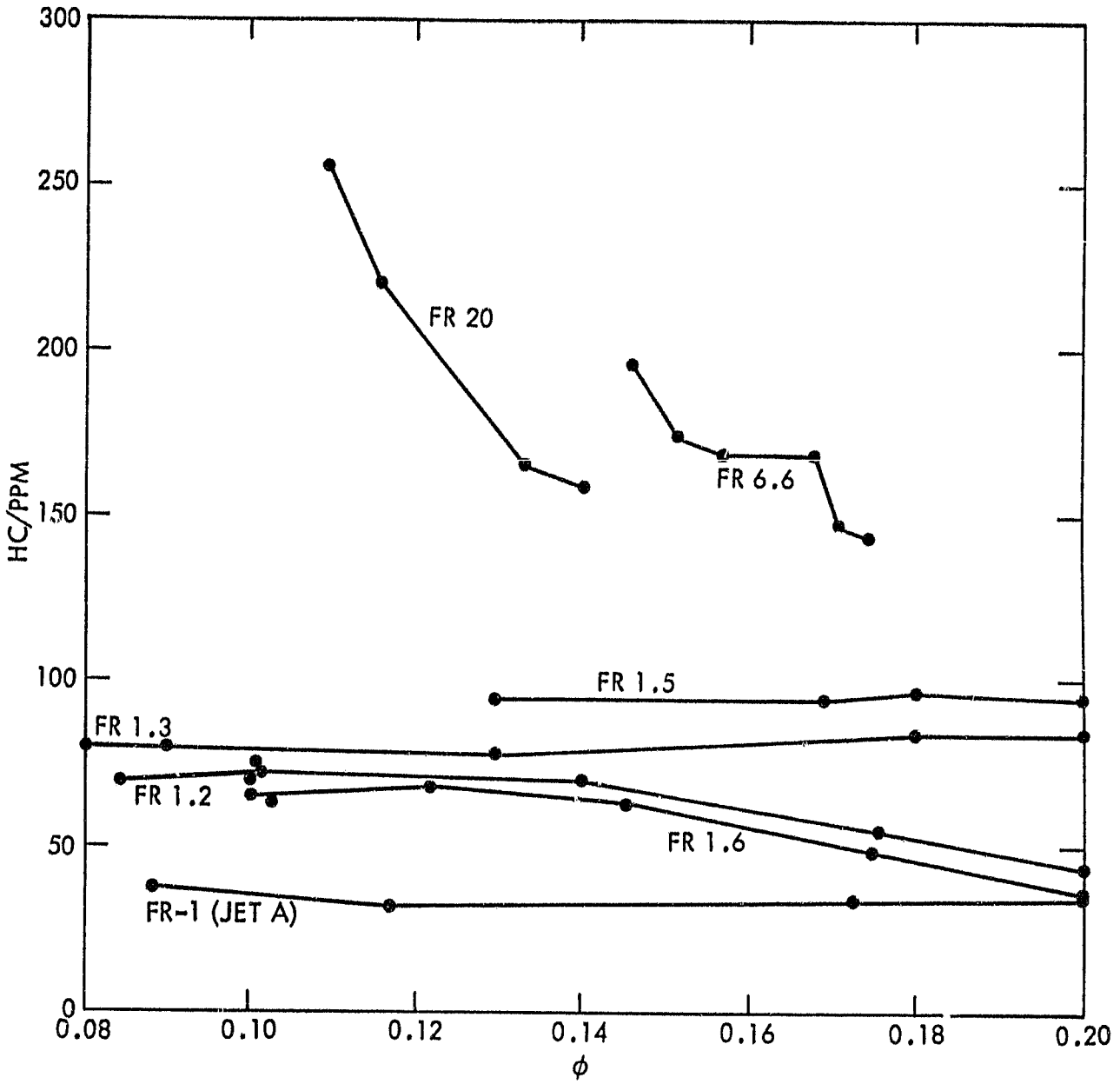

FIGURE 2-2. HYDROCARBON EMISSIONS MEASURED AT IDLE CONDITIONS

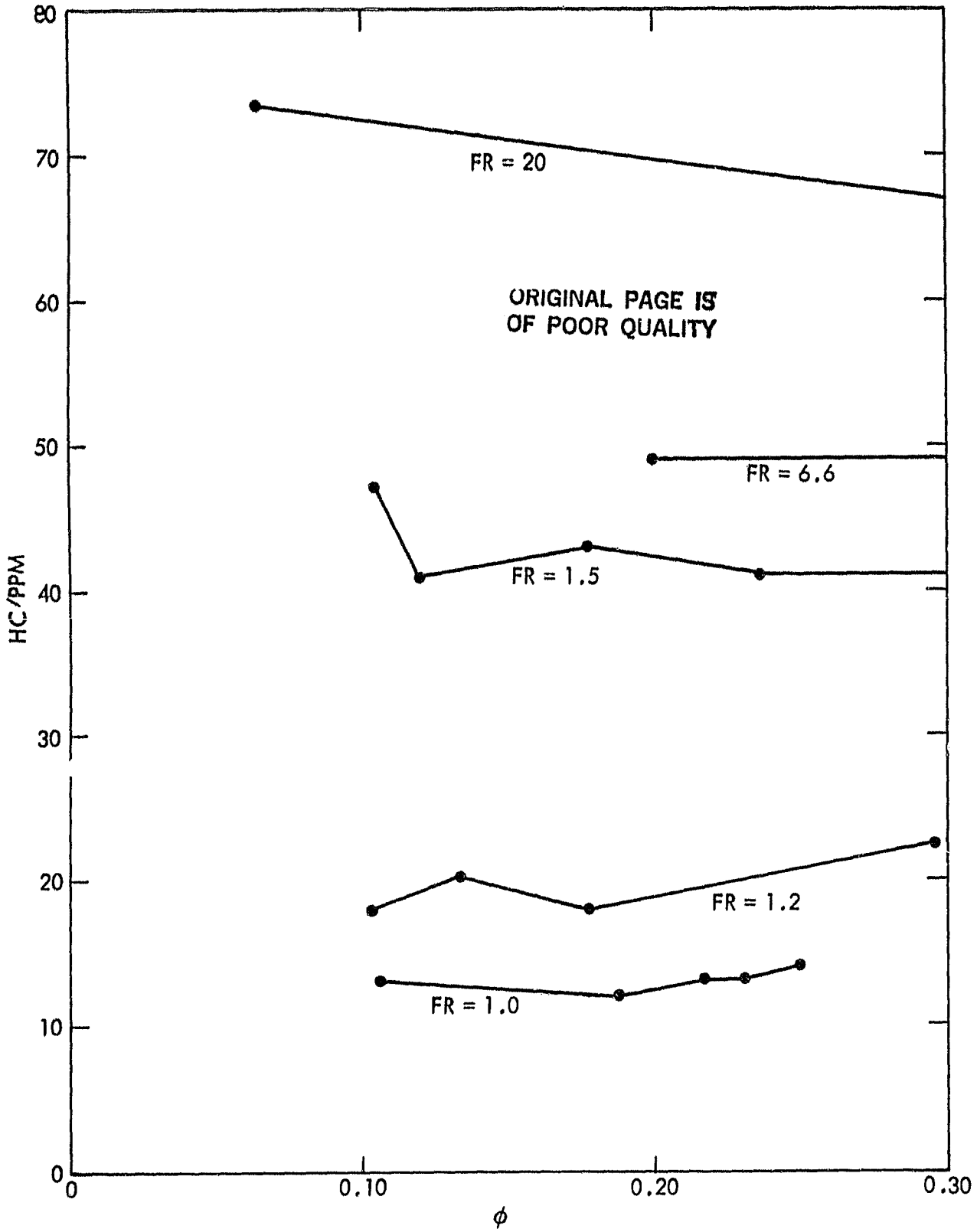

Figure 2-3 HYDROCARBON EMISSIONS MEASURED AT CRUISE CONDITIONS

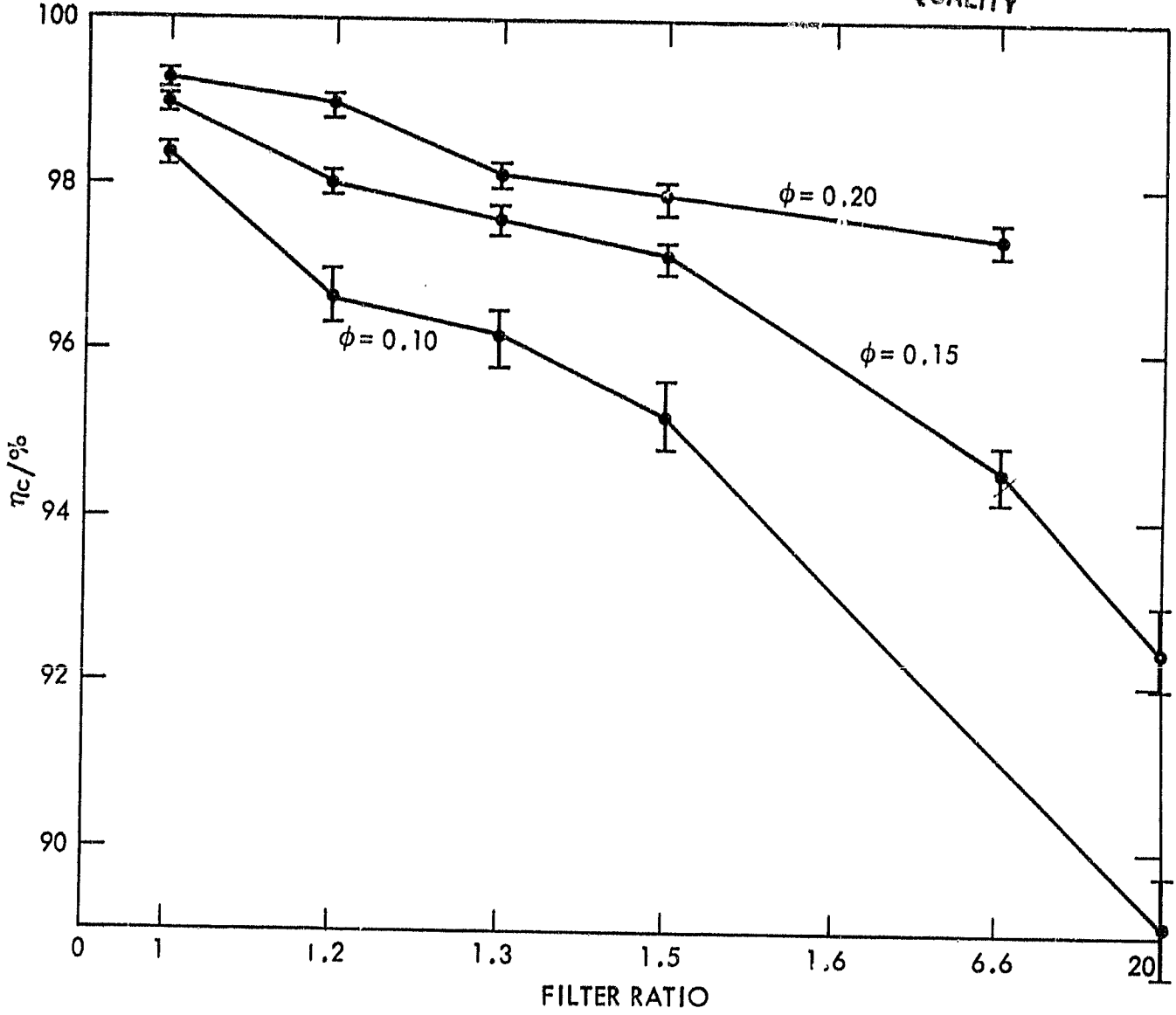

Figure 2-4 COMBUSTION EFFICIENCY, η_c, AT IDLE CONDITIONS AS A FUNCTION OF FILTER RATIO

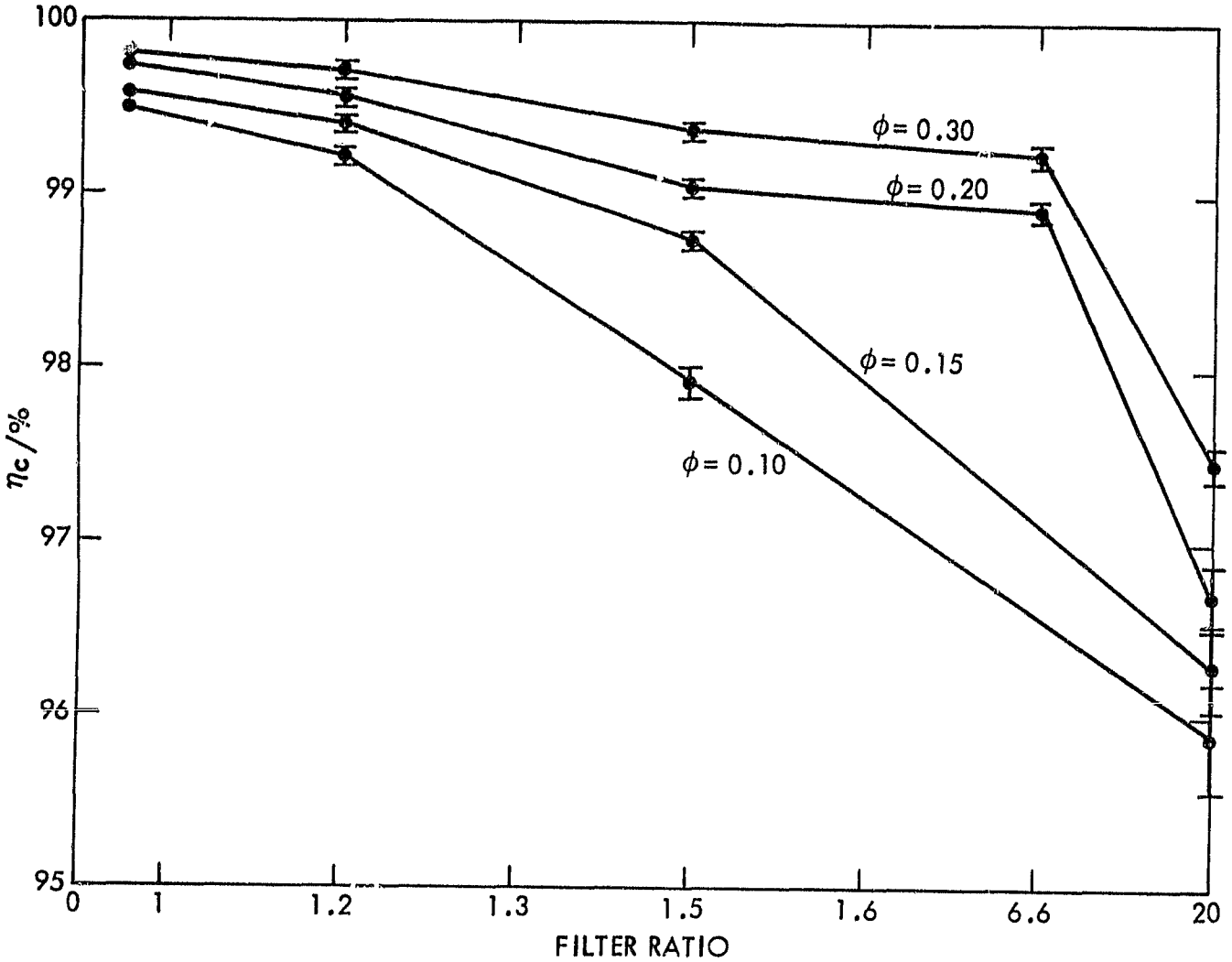

Figure 2-5 COMBUSTION EFFICIENCY, η_c, AT CRUISE CONDITIONS AS A FUNCTION OF FILTER RATIO

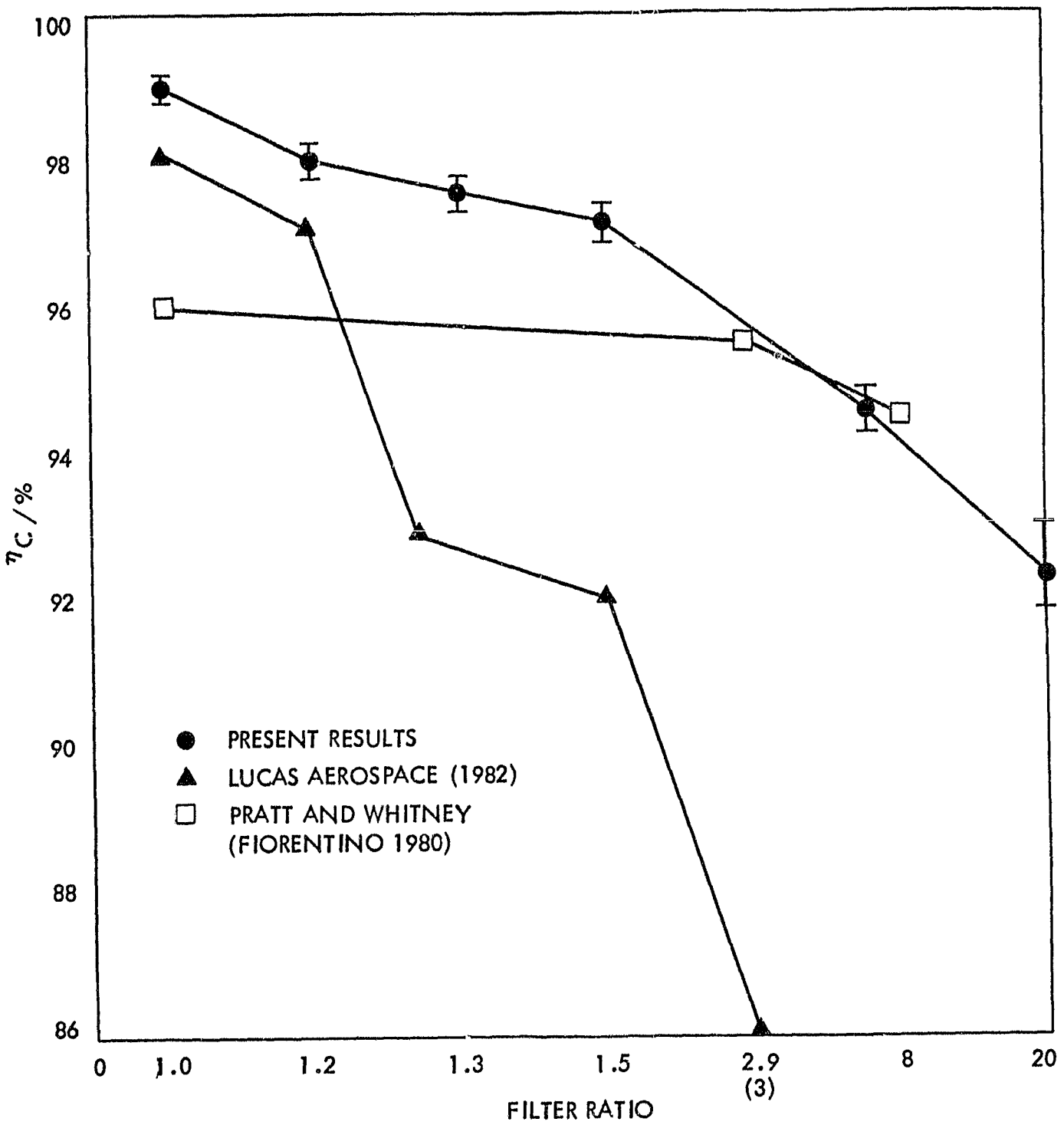

Figure 2-6 COMPARISON OF THE PRESENT RESULTS WITH THOSE OF LUCAS AEROSPACE (1982) AND PRATT & WHITNEY (FIORENTIONO, 1980). (JPL AND LUCAS RESULTS AT ϕ=0.15, P&W RESULTS AT ϕ=0.18)

Table 2-11 Lean Limit Test Results

Fuel	Filter Ratio	$\dot{m}_a$ kg/s	$\dot{m}_f$ g/s	A/F Ratio	ϕ	T_{plenum} °C
Jet A	1.0	0.620	1.32	470	0.032 ±0.01	40
AMK	1.2	0.608	0.696	874	0.017 ±0.01	130
AMK	1.3	0.640	1.40	460	0.032 ±0.01	185
AMK	1.5	0.622	2.00	311	0.048 ±0.01	170
AMK	6.6	0.640	7.5	85	0.174 ±0.02	150
AMK	20	0.626	10.5	60	0.250 ±0.03	178

These data are plotted in figure 2-7. A clear trend is evident indicating a strong sensitivity of the combustion margin to fuel degradation and atomization. The very slight upturn of the data to higher ϕ for Jet A is smaller than the uncertainty of the measurement and is the result of the cooler inlet air temperature of that test (40° C) compared with the others (nominally 160° C). The uncertainties indicated are derived from estimation of the accuracy with which the air and fuel flow rates were measured and from the uncertainty in precise determination of the blow out point due to combustion instability near the lean limit. Cooler temperatures inhibit fuel evaporation just as does reduced atomization, adversely affecting the lean limit.

One of the major goals of the research was to directly relate the engine combustion and atomization performance of the fuel. As outlined earlier this was accomplished through analysis of fuel nozzle sprays produced in a simulator operated at 22° C and 1 atm (14.1 Lb/in^2 absolute) pressure described in section 1 and through the combustion tests described in this section. The results of this effort are shown in figure 2-8 which presents achieved combustion efficiency as a function of spray SMD. To construct this figure, the SMD results as a function of filter ratio were linearly interpolated to yield the expected SMD at the filter ratios used for the combustion tests. Excellent correlation of the two quantities is observed for both idle and cruise conditions. The idle condition dependence is considerably stronger than that of the cruise condition. This is felt to be another manifestation of the inlet temperature effect on fuel evaporation discussed above. It is recalled that idle inlet temperature is nominally 120° C while cruise conditions call for an inlet temperature of nominally 350° C. At the relatively lower idle temperature, fuel vaporization necessary for efficient combustion is more sluggish so that the contribution of fine atomization to combustion efficiency is relatively more important. These results indicate clearly that in fact poor atomization is the direct basis for poor combustion performance of modified fuels. Figure 2-9 shows the lean limit data as a function of spray SMD. Here again a good correlation of combustion performance with fuel atomization is evident.

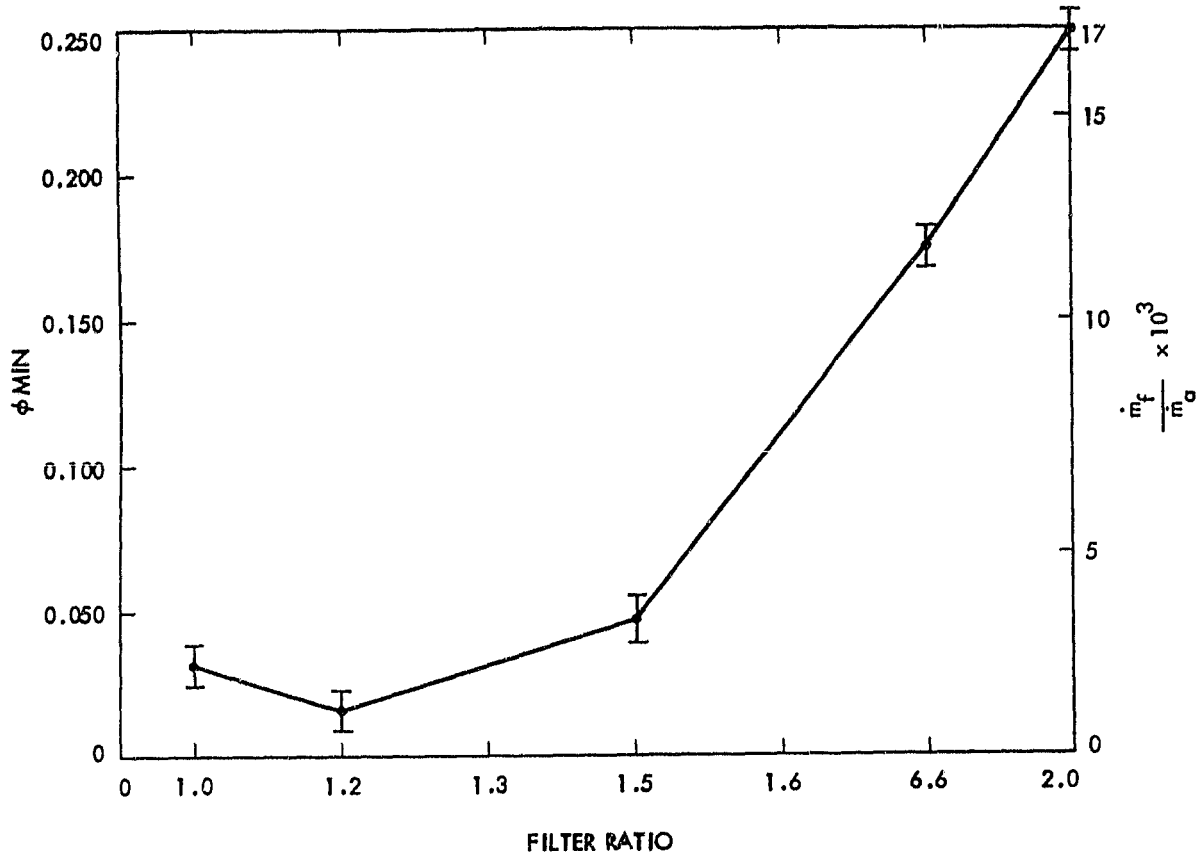

Figure 2-7 LEAN COMBUSTION LIMIT AS A FUNCTION OF FUEL FILTER RATIO

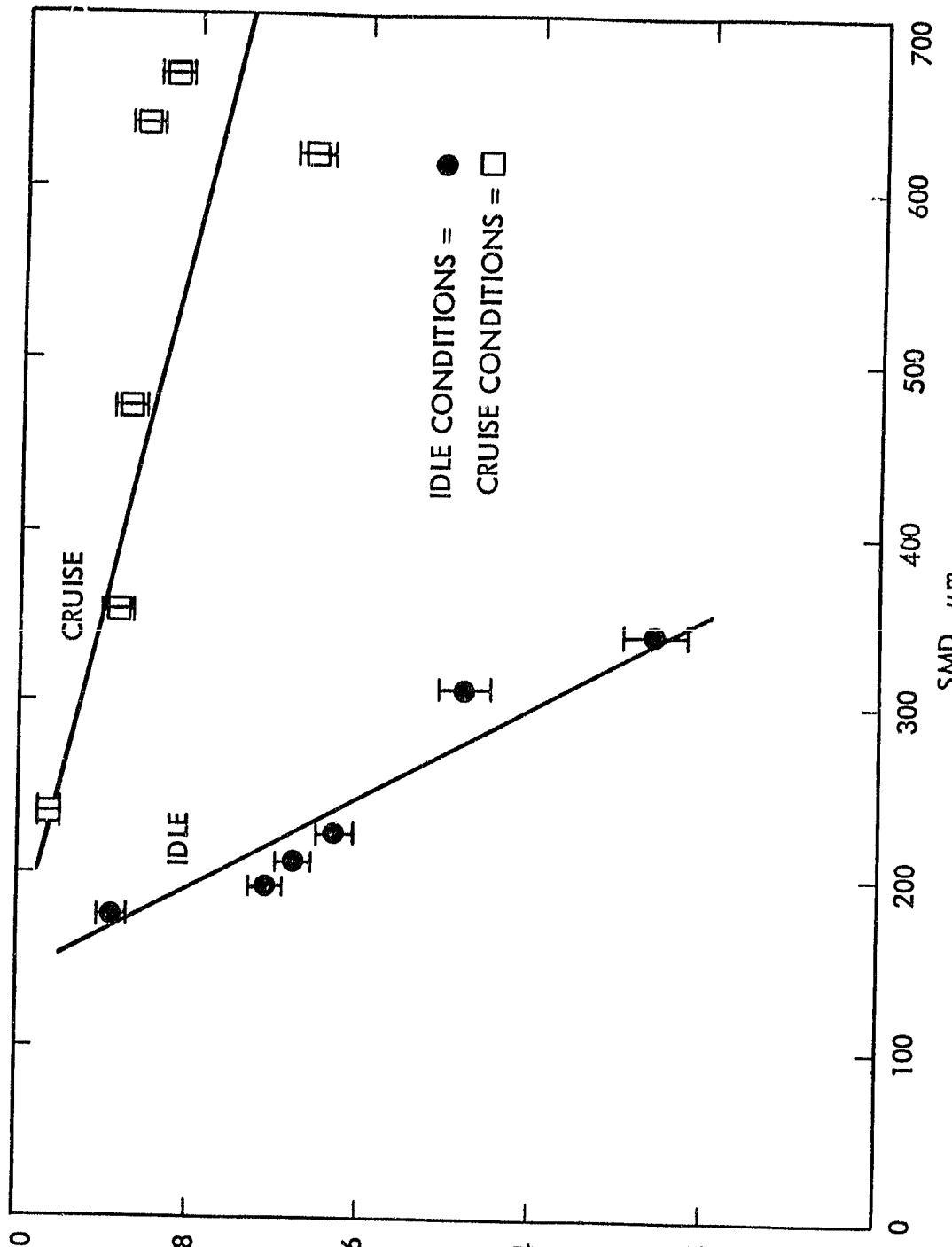

Figure 2-8 COMBUSTION EFFICIENCY, η_C, AT IDLE AND CRUISE CONDITIONS AS A FUNCTION OF THE FUEL SPRAY SMD

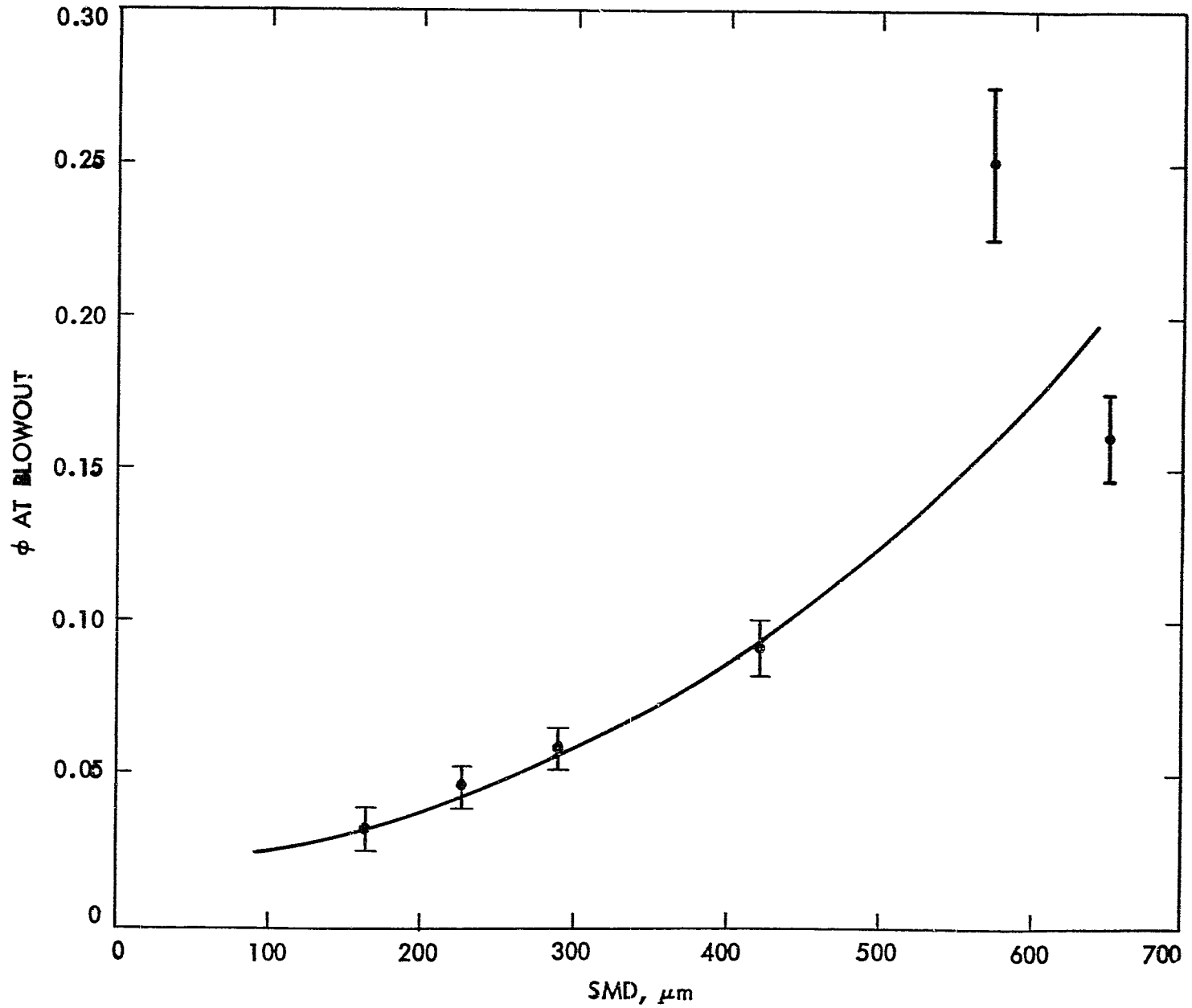

Figure 2-9 LEAN COMBUSTION LIMIT AS A FUNCTION OF THE FUEL SPRAY SMD

2.4 The Role of Fuel Heating

The concept, introduced in Appendix C, of fuel heating as a means of enhancing degradation might prove very beneficial in the light of the present results. In Appendix C it was shown that raising the temperature of the fuel by 20° to 50° C greatly increased the fuel's degradability for a fixed degrader orifice pressure drop. Filter ratio of the fuel was shown to decrease from 30 to 10.4 at 27° C and from 30 to 6.2 at 61° C using the same degrader operating conditions. Two additional benefits would be realized by fuel heating which are not reflected by this result. If the fuel were used in the engine at the elevated temperature achieved for its degradation, the fuel viscosity (and hence filter ratio) would be further decreased. This is due to the natural decrease in liquid viscosity with increasing temperature. Atomization is directly related to liquid viscosity, increasing as viscosity decreases so that use of heated fuel would certainly increase combustion efficiency. The role of increased temperature in speeding fuel vaporization has already been discussed. It has also been observed experimentally through the differing slopes of the cruise and idle data relating $_c$ with spray SMD. At idle, inlet temperatures are lower, so atomization is relatively more important as a mechanism for fuel vaporization than at higher (cruise) inlet temperatures. In figure 2-8, the idle results show a much stronger dependency on spray atomization than do the results at cruise. Heated fuel drops will evaporate more readily and raise combustion efficiency independently of the extent of atomization. Thus three benefits may be derived from fuel heating: increased degradation for a fixed degrader power level, decreased fuel viscosity and increased evaporation rates. A potential problem area associated with fuel heating may be the engine controller. Fuel temperature ranges are specified by engine manufacturers and are usually within a close tolerance. Fuel controllers are very sensitive to fuel temperature and an increase in the fuel temperature may seriously affect fuel controller performance and life. Further investigation of the possible benefits and means of implementation of the fuel heating concept in an engine system are recommended.

3. CONCLUSIONS

A) Atomization Performance

1) As the filter ratio was increased from 1 (Jet A) to 2.8, the spray SMD increased from 160 to 390 μm at ignition, from 175 to 215 μm at idle, from 235 to 665 μm at cruise, and from 225 to 380 μm at take-off (see Table 3-2).

2) Artificial limitation of the spray characterization system range to drops of diameter less than 500 μm yields results very similar to those obtained by other workers (Reference 4) using laser scattering devices. This result demonstrates the importance of accounting larger fuel masses to the accurate characterization of AMK sprays.

B) Combustion Performance: Ignition Conditions

1) Lean blow out occurred at ϕ = 0.032 for Jet A and increased to ϕ = 0.250 for AMK of filter ratio 20. This correlated with a spray SMD increase from 161 μm for Jet A to approximately 600 μm for AMK of filter ratio 20.

2) Lean blow out equivalency ratio correlated directly with SMD, increasing from 0.035 at an SMD of 115 μm to 0.16 at an SMD of 650 μm.

C) Combustion Performance: Idle Conditions

1) Combustion efficiency dropped from 99.3 percent for Jet A at ϕ = 0.20 to 99.0 percent at ϕ = 0.20 for AMK of filter ratio 1.2 and to 97.9 percent for AMK of filter ratio 1.5 at ϕ = 0.20. At ϕ = 0.10, Jet A η_c was 98.4 percent which dropped to 96.7 percent for AMK of filter ratio 1.2 and to 96.2 percent for AMK of filter ratio 1.5. At a filter ratio of 20, η_c dropped to 89 percent for ϕ = 0.10.

2) Combustion efficiency was inversely related to cold spray SMD, decreasing from an average 98.7 percent at an SMD of 175 μm to 92.6 percent at an SMD of 335 μm.

D) Combustion Performance: Cruise Conditions

1) Combustion efficiency dropped at ϕ = 0.30 from 99.8 percent for Jet A to 99.7 percent for AMK of filter ratio 1.2. At filter ratio 1.5 η_c was 99.4 percent; at filter ratio 6.6 η_c was 99.3 percent, and at filter ratio 20, η_c was 97.5 percent. Combustion efficiency also dropped for each filter ratio fuel with decreasing ϕ. For example, for AMK of filter ratio 1.5, η_c was 99.4 percent at ϕ = 0.30, 99.1 percent at ϕ = 0.20, and 97.9 percent for ϕ = 0.10.

2) Combustion efficiency was inversely related to cold spray SMD decreasing from an average 99.6 percent with an SMD of 235 μm to 97.5 percent at an SMD of 675 μm.

E) Degrader Performance

1) The needle valve degrader of Mannheimer requires more than one pass with a pressure drop of 135 atm (2000 lb/in^2) to reach a fuel filter ratio of 1.2. Higher pressure drop should achieve the required degradation.

2) Heating of the fuel before degradation by 34° C resulted in a filter ratio drop via degradation of 24 (from 30 to 6) compared to a drop of 20 (from 30 to 10) without heating.

References

1. Fleeter, R., Petersen, R.A., Toaz, R.D., Jakub, A., and Sarohia, V. (1981), "Antimisting Kerosene Atomization and Flammability", Interim Report, U.S. Department of Transportation, Federal Aviation Administration.

2. Fleeter, R., Toaz, R.D. and Sarohia, V. (1982), "Application of Digital Image Analysis Techniques to Antimisting Fuel Spray Characterization". To be presented at ASME 1982 Winter Annual Meeting, Phoenix, AZ.

3. Mannheimer, R.J. (1982), "Degradation and Characterization of Antimisting Kerosene", Final Report, U.S. Department of Transportation, Federal Aviation Administration Report No. DOT/FAA/CT-82/93.

4. Fiorentino, A., DeSaro, R., and Franz, T. (1980), "An Assessment of the Use of Antimisting Fuel in Turbofan Engines", Pratt & Whitney report No. PWA 5097-29, NASA report No. CR-165258, December 1980.

5. Lucas Aerospace (1982), "An Assessment of the Performance of an RB211 Combustor Using Antimisting Kerosene (FM-9)", Report No. B 49 556.

6. Yavrouian, A., Sarbolouki, M., and Sarohia, V. (1981), "Influence of Liquid Water and Water Vapor on Antimisting Kerosene (AMK)", U.S. Department of Transportation, Federal Aviation Administration (to be published).

7. Knight, J. (1981), "Modified Filtration Ratio Test Procedure for AMK", R.A.E. Note, November 1981.

8. Pratt & Whitney (1982), NASA/P & WA Antimisting Fuel Program Review, June 1982.

APPENDIX A: System for Digital Analysis of Spray Images

Processing system architecture is depicted by figure A-1. Image acquisition, display and basic processing is performed with a DeAnza ID-5400 Image Display System. The hardware package includes a vidicon and power supply for analogue image formation, 3 image refresh memory channels, a digital video processor, and a color video monitor. The processor contains a signal digitizer which writes an analogue vidicon frame onto one of the memory planes as a 512 x 512 x 8-bit digital image, as well as hardware to perform arithmetic functions on 2 images in the refresh memory at video rates (30 frames per second). From a starting image such as figure 3-3 showing typically 100 cm^2 of the spray, a group of subimages each covering approximately 10 mm^2 of the spray is formed.

This digitization of the analogue image is carried out on a light table with a vidicon and image digitizer (DeAnza ID-5400) operating in conjunction with a host minicomputer (PDP 11/34). With this system an image composed of 512 x 512 digital picture elements (pixels) is recorded in hardware memory (RAM) from the analogue signal of the vidicon. Each matrix element is an 8-bit number (0 to 255) corresponding to the image brightness at that point. While digitization can proceed at video rates (30 frames per second), a program is used which creates one digital image from the average of 64 consecutive digitized frames. The image thus formed suppresses the random noise present in the vidicon signal and the digitizer electronics. A copy of this digital image in the video digitizer memory is copied onto a disk file of the PDP-11/34 computer which acts as a host to the DeAnza system.

Magnification of the photographic image onto the vidicon is adjusted so that the analogue resolution is equated with the digital resolution. The pixel size is thus equated with the specified equivalent line width of the film (3 μm). Thus a 512 x 512 pixel image corresponds to 1.5 x 1.5 mm on the film. This, in turn, means that a single digital image records a portion of the spray approximately 3 x 3 mm square. At this image scale a 2 mm diameter drop may be recognized in the same field as an 8 μm diameter drop. The instrument dynamic range thus spans a factor of 250 diameters.

Fundamental to the image processing phase of the research is the recognition/detection scheme for individual fuel drops in the imagery. Scattering of the laser light by the fuel produces consistent drop intensity profiles characterized by sharp brightness gradients at the drop edges and relatively constant brightness values throughout the drop interior. In order to isolate drops with this type of signature from the scene background and noise from sources such as film grain and artifacts of the analogue to digital conversion process, thresholding was applied to the original image. By selecting as a threshold for each complete subimage one of the 256 possible gray levels, the original DN (digital number) of each image pixel will be set to 255 or 0 depending on whether it falls above or below the threshold. Those pixels equal to or exceeding the threshold are assumed to constitute part of a fuel drop. Adjoining above-threshold pixels are then combined to define a single drop whose characteristics are reported to the analyst.

While various image preprocessing enhancement measures were considered, the strong drop signature resolved from thresholding made detailed enhancement

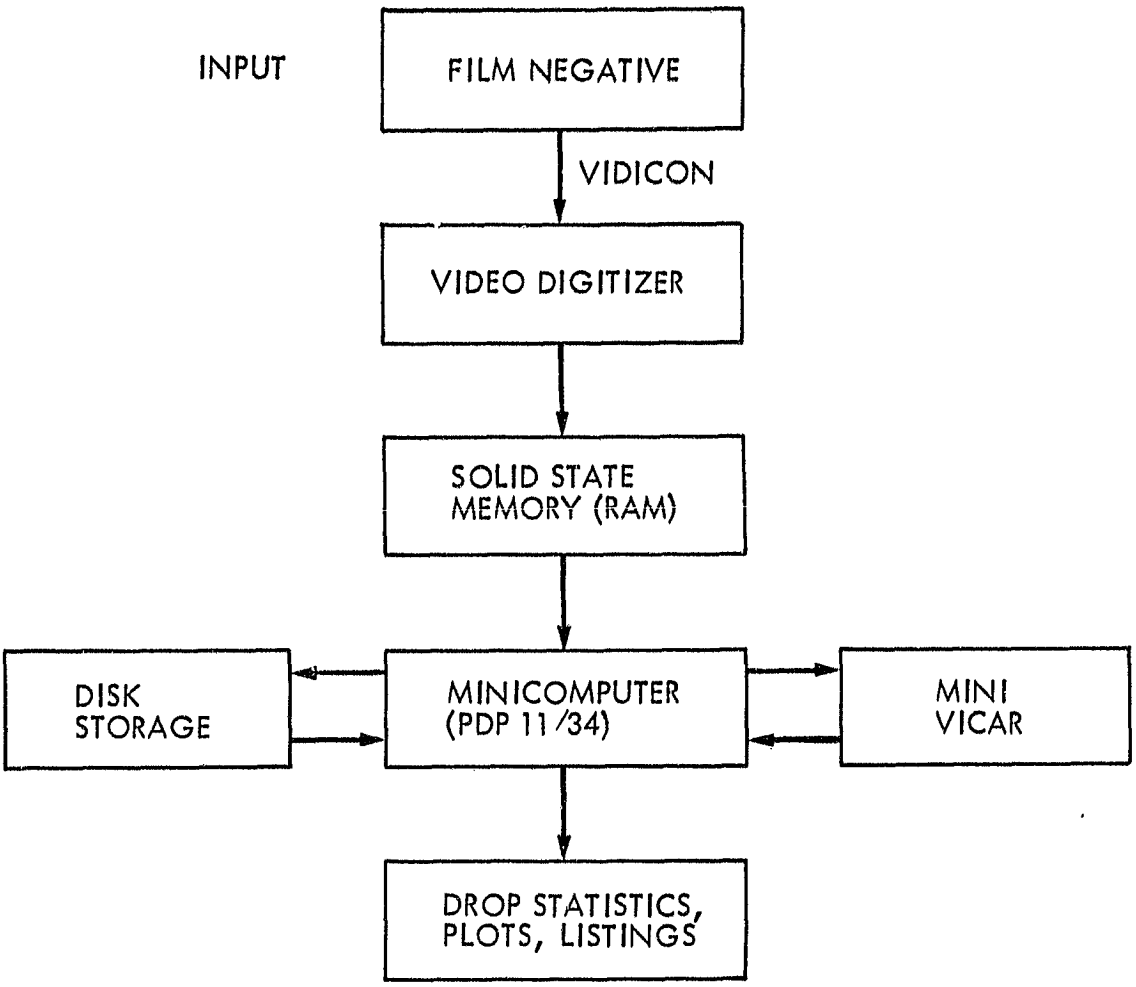

FIGURE A-1 . DIGITAL IMAGE PROCESSING SYSTEM ARCHITECTURE

unnecessary. Elimination of high frequency noise generated by film grain and aliasing in A/D conversion was the only such step taken. Aliasing is the generation of spurious signals by sampling high frequency data at too low a sampling frequency. This filtering was accomplished simply by limiting the smallest drop counted to an area of 5 pixels, thus eliminating random above-threshold 'noise' pixels.

Software operations on the image processing system are divided into 2 categories. Images residing in the refresh memory of the DeAnza are processed with software that operates through a Direct Memory Access (DMA) interface in which the PDP-11 sends and receives data from the DeAnza memory and its registers via a DeAnza driver program. The vidicon image display, averaging and storage capability is part of this DMA interface software. An addition to these programs, interactive thresholding, is achieved by passing one of the 3 digital image memory channels through a hardware lookup table as it is sent to the video monitor, allowing the analyst to view a wide range of image thresholds quickly. The other category of software operations is installed on the PDP 11/34 host computer and is based on a JPL-developed software package known as MINI-VICAR. The MINI-VICAR standard algorithms for digital image management have been augmented with programs specific to the mist analysis application. MINI-VICAR works in conjunction with the host operating system (in this case, RSX-11M Version 3.2) to provide efficient image retrieval and I/O functions for the image data. Included in the package is a library of applications software to provide fundamental image processing operations such as pixel DN histogram generation, contrast enhancement, filtering, mosaicking, etc. For the specific purpose of the research described in this paper, a drop counting program was added to the MINI-VICAR software to perform the threshold-based drop detection process. This program scans the image in a raster format, flagging pixel strings satisfying the current threshold value as 1-dimensional droplet segments. For succeeding lines, adjoining segments are concatenated and their area and image coordinate location are consolidated to represent a single, larger drop. As each drop is completed, its parameters are reported to the analyst on the video terminal, or optionally queued to a disk data set and printed at the line printer. Processing time is less than 1 minute per subimage.

For this study, the images were used to provide a measure of individual drop cross sectional area. In order to express these data in the customary form of a diameter measure, the cross sectional area was considered to be that of a sphere and the diameter of this representative sphere was calculated. Drop data accumulated in the disk data set is then used to calculate spray parameters and to form drop size histograms.

To analyze a spray, a group of 512 x 512 pixel subimages is normally analyzed. Selection of samples from the negative depends on the information desired. For statistics generated over the whole spray field, the negative is sampled at wide horizontal and vertical increments so that sampling occurs over the entire image. Alternatively, data may be derived, for example, at only 1 axial location in the spray field by sampling radially at that axial location. To gain information at just one location, subimages are clustered about the spray region of interest. This flexibility is made possible by generation of a photographic record and by vidicon digitization. The computer operator manipulates the vidicon and light table interactively with the computer to follow whatever sampling strategy may be indicated.

APPENDIX B: Testing the Drop Measurement System Accuracy

The accuracy of the drop measuring technique has been tested by independent measurement of size distributions of glass spheres. A sample of the spheres was characterized first by microphotography and then by measurement of the sphere image size manually with a micrometer. A histogram composed of over 500 sphere measurements was created. A new sample was then deposited on a glass slide and counted using the digital imaging technique. The results are compared in figure B-1 and Table B-1. Results of mean size and SMD are in agreement within about 2 μm, which is the accuracy with which the relationship between image size and viewing field size can be established at the magnification used (2.52 μm per pixel or a viewing field of 1.6 mm^2).

Table B-1. Accuracy Test of the Drop Counting Algorithm: Glass Bead Analysis

	Manual Counting	Computer Counting
Number Counted	549	305
Mean Diameter/μm	132	130
(Mean Diameter)^2/μm^2	17,500	16,900
SMD/μm	133	132

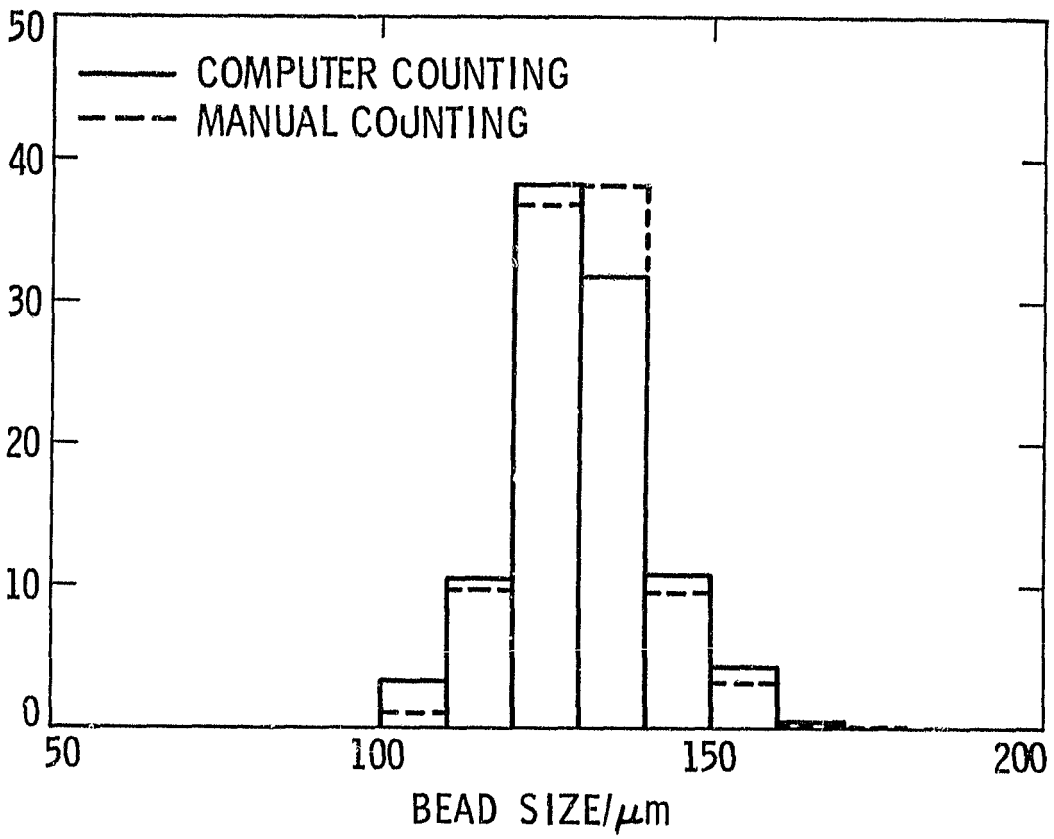

FIGURE B-1. COMPARISON OF RESULTS FROM MANUAL AND COMPUTER COMPOSITION OF STATISTICS ON GLASS BEAD DIAMETERS

APPENDIX C: FUEL DEGRADATION AND CHARACTERIZATION

C.1 Measurement of Fuel Degradation Level

It is unfortunate that so much of the effort in degradation is aimed at lowered filter ratio test results. The goal of degradation is ultimately not to enhance fuel flow rate through fine filters but rather to restore atomization performance. While in section 1 a direct link was demonstrated between filter ratio and atomization, this may not be true in all cases. Fuels degraded by different techniques may show identical filter ratios but differing spray qualities. Increased water content in the fuel raises the filter ratio dramatically (Reference 6) but may not diminish atomization or combustion performance significantly.

Very little has actually been accomplished to ameliorate these problems. JPL has suggested indirect measurement of fuel atomization as a degradation measure. Degradation level in terms of atomization performance could thus be determined. To the degree such a measurement may be easily and rapidly performed, this technique appears to offer significant advantages. This method is not available for widespread use at present.

Currently, the most widely accepted and applied technique for characterization of AMK degradation level is the filter ratio test. This is the measure reported for description of the fuel used in this work. The ratio of the time of passage of a specific quantity of the subject fuel through a filter to the time for the same quantity of Jet A to pass through the filter under specific conditions is the basis of the measure. It is described in detail in the step-by-step description below and figure C-1.

C.2 Degradation Method

By breaking the polymer additive molecules into smaller segments it is possible to largely restore the viscous properties of AMK to those of the Jet A from which it was blended. Because of the very large size of the molecules, this reduction in polymer size may be accomplished simply through mechanical stress such as that applied to the fluid in a blender or in passing through a small tube or orifice. While various mechanisms have been designed for this purpose, very few are continuous, rapid flow devices which may be used to degrade the large amount of fuel (~ 100 liters) needed for combustion tests. The apparatus first devised by Mannheimer (Reference 3) was used because it is capable of relatively high degradation levels (filter ratio < 2) and the rate of fuel degradation is limited only by the pump used to drive the fuel through the degrader. The apparatus is shown schematically in figure C-2 and consists of a reservoir of undegraded fuel and a high pressure, air driven pump which forces the fuel through a needle valve. The needle valve may be progressively closed with the pump operating until a predetermined pressure drop exists across it. Since this pressure drop occurs because of viscous dissipation in the fuel the degree of degradation is roughly proportional to the pressure drop. A reservoir charged with high pressure nitrogen is provided between the pump and the needle valve. This serves to dampen pressure fluctuations across the valve which occur with the cyclic motion of the pump diaphragm. At 135 atm pressure drop, fluctuations were below 5 atm. On a typical 3500 lb/in^2 gauge the fluctuations are only barely visible.

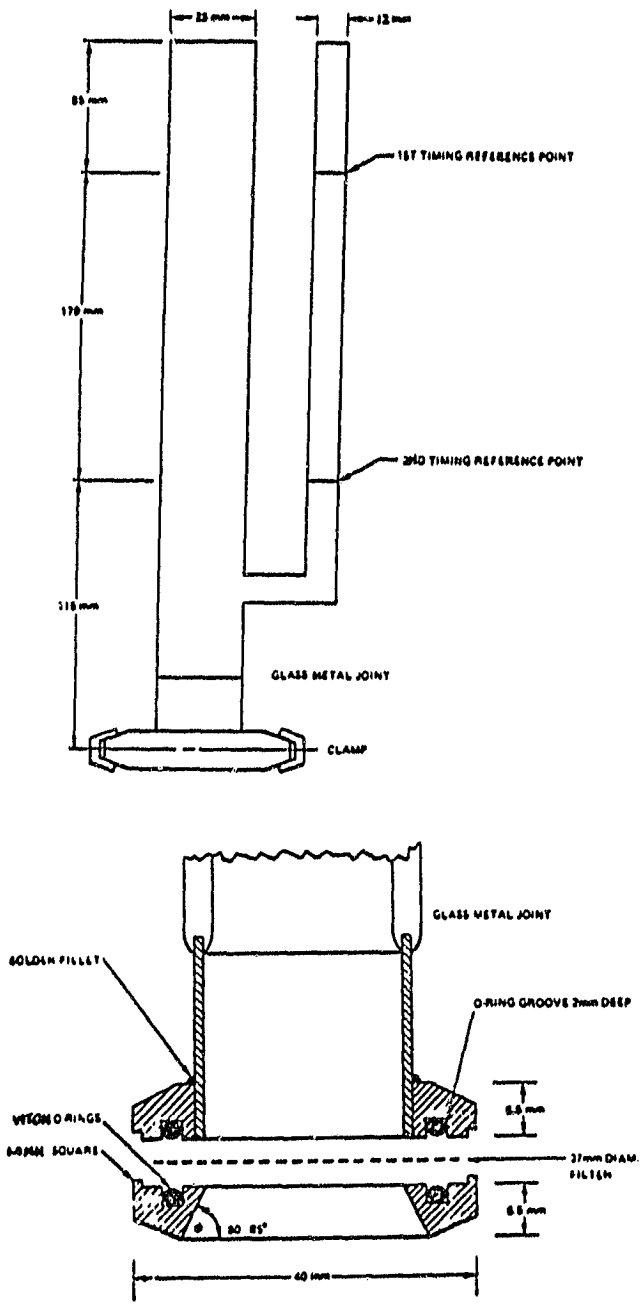

FIGURE C-1. THE FILTER RATIO TEST APPARATUS

Description of Filter Ratio Test

Fuel temperatures for Jet A and AMK are 20 ±1° C.

Apparatus: Filtration ratio apparatus as shown in Fig. C-1

Type of filter used: 16 - 18μ twilled Dutch weave stainless steel 164 x 1400 mesh cloth, warp diameter 0.07 mm and weft diameter 0.04 mm, pre-cut into discs of 44.5 mm diameter. The material is obtained from Tetco, Inc., 525 Montery Pass Road, Monterey Park, CA 91754.

1. Make sure filter apparatus has been rinsed clean with Jet A and then drained. Residual AMK can influence the filter time of the next sample.

2. Place an unused filter on lower filter plate, positioning it in the center so that it overlaps the edge of the orifice.

3. Both 'O' rings should be properly seated. Align upper and lower filter plates the same way each time; attach lower to upper and apply screws, tightening them to the same tolerance each time.

4. Insert a rubber stopper in bottom orifice, choosing a size which does not contact the filter. Hold stopper steady until removal. Excess motion may induce gelation in the filter.

5. Tilt apparatus to diagonal and pour the reference Jet A slowly down side of tube.

6. Once tube is about 3/4 filled, return it to vertical, add fuel till it overflows into gallery.

7. Remove rubber stopper. Record time between timing reference points.

8. When apparatus has drained, replace stopper, tilt apparatus to diagonal and pour sample AMK slowly (90 seconds) down side of tube, not letting it hit bottom directly.

9. Repeat step 6.

Tests on the degrader assembled at JPL showed that a pressure drop of 135 atm (~ 2000 lb/in^2) results in a reduction of the filter ratio from 30 (undegraded) to 3.4. A second pass of this fuel at the same ΔP yields a filter ratio of 1.3. Beginning with partially degraded fuel (filter ratio 20) the same pressure drop also yields an output filter ratio of 1.3. In no case was a filter ratio under 1.3 observed with fuel degraded solely with this degrader. This may be an inherent limitation if the pressure drop is limited to 135 atm. Tests at higher pressure differentials (up to 240 atm [~ 3500 lb/in^2]) should be carried out to verify this supposition.

C.3 Temperature Effects on Degradation

Because the antimisting polymer will also break down at elevated temperatures, an investigation was undertaken to determine whether degradation could be enhanced by first elevating fuel temperature. The results of these tests are shown in Table C-1. In all tests, fuel temperature was returned to 20° C before performance of the filter ratio test. A highly degraded case was examined by starting with partially degraded fuel (filter ratio 21.5) and using the maximum available pressure drop (135 atm). Here the effect is harder to see because the limit of resolution of the filter ratio test itself is being approached. However a 10° C elevation in temperature from 26° C to 36° C yields fuel 17 percent closer to the ideal filter ratio of 1.0. To operate in a regime where the filter ratio test is more sensitive a lower degradation level was also attempted. This would correspond (due to the lower ΔP used) to a smaller, lighter and less power consuming degrader. In this regard it is noted that energy for running a more powerful degrader will be subtracted directly from the available engine shaft available power. On the other hand, energy for heating of the fuel may be available from waste heat and would not affect the power output available at the engine. An additional benefit to heating the fuel is that fuel viscosity is lowered at elevated temperature. This will likely enhance atomization. Fuel combustion would be enhanced not only by the improved atomization but also because warmer fuel will evaporate more readily upon initial injection into the combustion region, resulting in more rapid and efficient combustion. From Table C-1 we see that the degradation levels achieved by this simulated low power consumption degrader are considerably lowered as the fuel temperature is increased. For each 10° C of temperature rise, a 20 percent decrease in degradation level as measured by the filter ratio was observed. By raising fuel temperature to 61° C it was possible to achieve a filter ratio of 6.2 with 1 pass at 35 atm pressure drop. Through further testing it was found that to degrade fuel of temperature 22° C to this filter ratio, a single pass at 70 atm was required. Since the degrader energy consumption to degrade a fixed amount of fuel is directly proportional to the pressure drop used, heating of the fuel in this case has cut degrader energy consumption by one-half. Fuel heating may potentially present problems with engine fuel controller as discussed on page 32 of this report and may require a controller redesign.

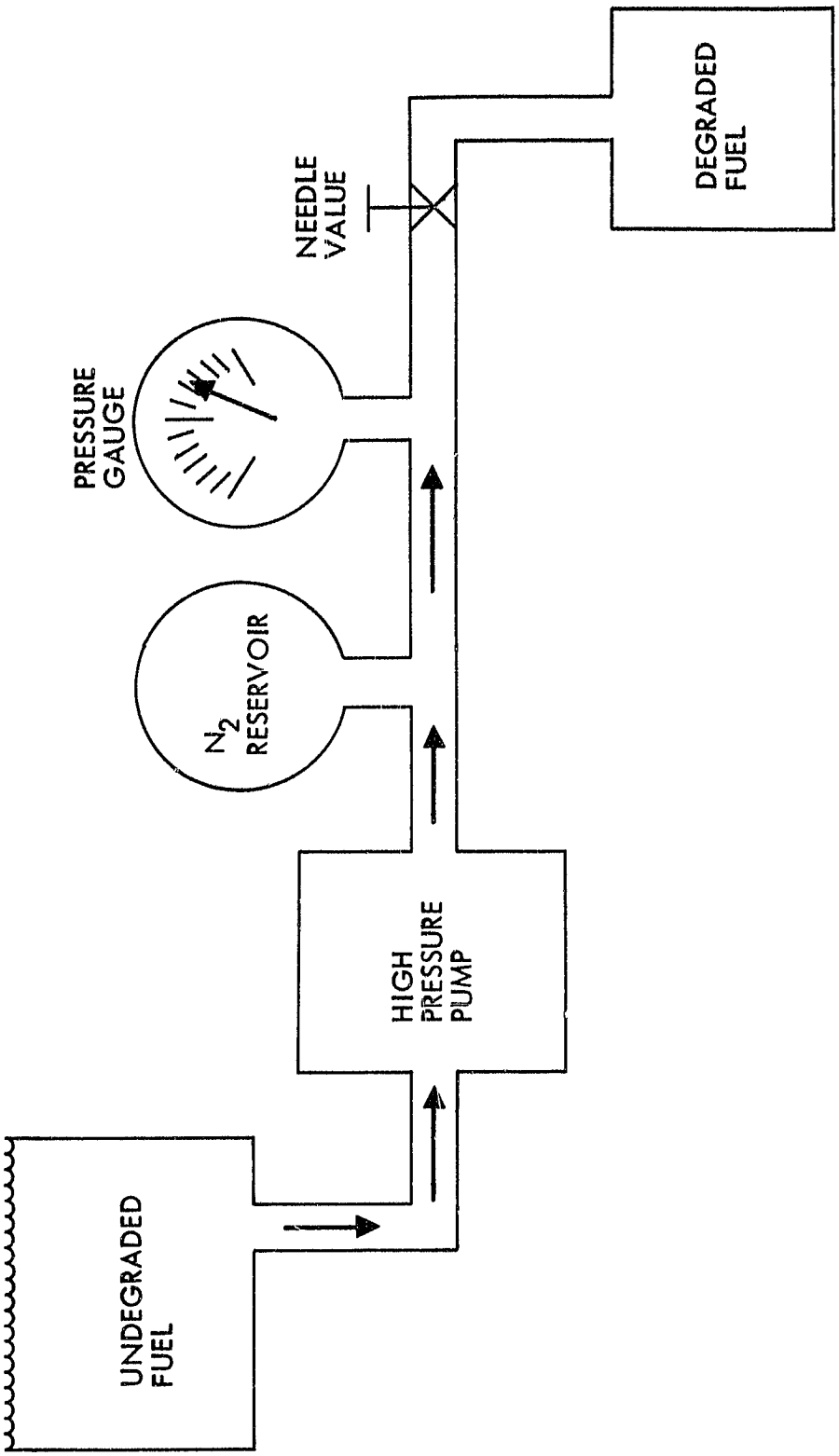

FIGURE C-2. SCHEMATIC DIAGRAM OF THE CONTINUOUS FLOW, NEEDLE VALVE DEGRADER

Table C-1. Degradation at Elevated Fuel Temperature

Filter Ratio Before Degradation	ΔP Across Degrader, Atm	Fuel Temperature, °C	Filter Ratio After Degradation (Fuel Temperature Returned to 20° C)
21.5	135	26	1.32
21.5	135	36	1.27
21.5	135	46	1.28
21.5	135	56	1.30
21.5	135	66	1.28
21.5	0	66	20.8
30	35	27	10.4
30	35	34	9.3
30	35	42	7.7
30	35	50	6.6
30	35	61	6.2
30	135	61	2.1

APPENDIX D

Method of Combustion Efficiency Calculation from Hydrocarbon Emissions Data

Combustion efficiency, η_c, is a number ranging from 0 to 1 (0 to 100 percent meant to express the fraction of the total fuel introduced into the combustion chamber which burns. Since the sum of the unburned fuel flow rate in the exhaust, m_{f1}, and the rate of fuel consumption by combustion, m_{f2}, must equal the rate of fuel injection, m_{f0}, we see that

$$\eta_c = \frac{\dot{m}_{f2}}{m_{f0}} = 1 - \frac{\dot{m}_{f1}}{m_{f0}} . \tag{1}$$

The hydrocarbon analyzer provides an indirect measurement of $\dot{m}_{f1}$. It does this by measuring the fraction of the exhaust (in parts per million) which consists of unburned hydrocarbons. The analyzer was calibrated using Hexane, hence a reading of 1 ppm means that material with the same amount of carbon as 1 mole of Hexane exists in the exhaust for every 10^6 moles of carrier gas. The assumption is made that the carrier gas is air. This is a reasonable assumption at the equivalency ratio used in the tests ($0.10 \leq \phi \leq 0.30$). Since the air mass flow rate is known (via its flow upstream of the combustor through a sonic orifice) the mass flow of equivalent Hexane is given simply by

$$\dot{m}_{Hex} = \dot{m}_{air} \frac{PPM_{Hex}}{1 \times 10^6} \frac{M_{Hex}}{M_{air}} \tag{2}$$

where M_{Hex} and M_{air} are the mole weights of equivalent Hexane and air, respectively. Equations (1) and (2) allow calculation of η_c as m_{Hex} is equated with m_{f1},

$$\eta_c = 1 - \frac{\dot{m}_{air}}{\dot{m}_{f0}} \frac{PPM_{Hex}}{1 \times 10^6} \frac{M_{Hex}}{M_{air}} . \tag{3}$$